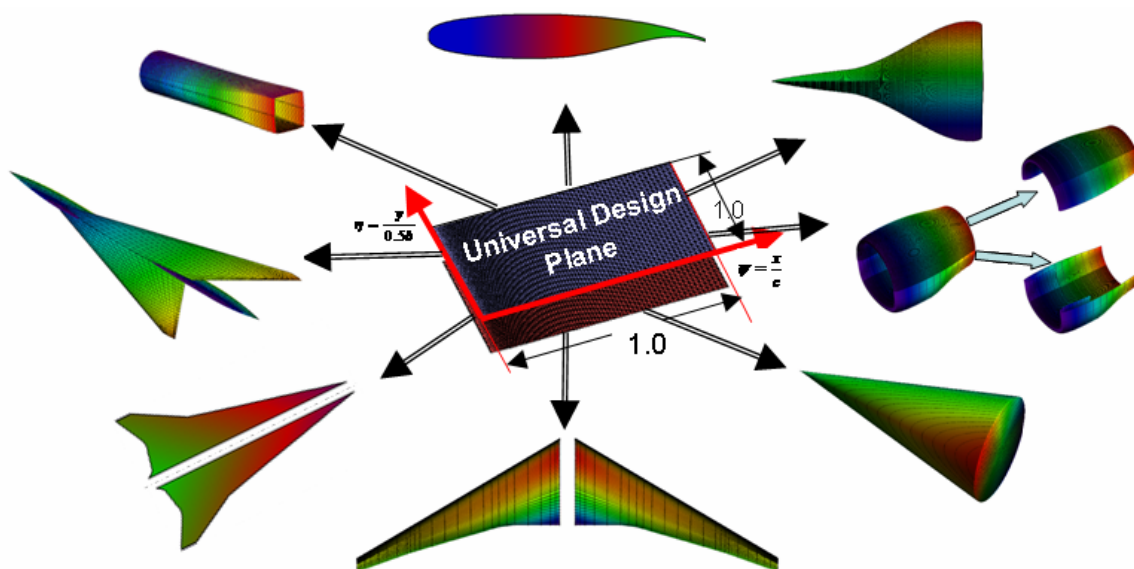


Modification of AIAA-2007-0062 & AIAA-2007-7709

The “CST” Universal Parametric Geometry Representation Method, Recent Extensions and Applications

Brenda M. Kulfan

Boeing Commercial Airplanes, Seattle, Washington, 98124



Royal Aeronautical Society Conference

AERODYNAMIC DRAG PREDICTION AND REDUCTION: CAPABILITIES AND FUTURE REQUIREMENTS

Tuesday 23rd – Wednesday 24th October 2007

No.4 Hamilton Place, London

Recent Extensions and Applications of the “CST” Universal Parametric Geometry Representation Method

Brenda M. Kulfan*

Boeing Commercial Airplanes, Seattle, Washington, 98124

For aerodynamic design optimization as well as for multidisciplinary design optimization studies, it is very desirable to limit the number of the geometric design variables. In reference 1, a “fundamental” parametric airfoil geometry representation method was presented. The method included the introduction of a geometric “class function / shape function” transformation technique, CST, such that round nose / sharp aft end geometries as well as other classes of geometries could be represented exactly by analytic well behaved and simple mathematical functions having easily observed physical features. The CST method was shown to describe an essentially limitless design space composed entirely of analytically smooth geometries. In reference 2, the CST methodology was extended to more general three dimensional applications such as wing, body, ducts and nacelles. It was shown that any general 3D geometry can be represented by a distribution of fundamental shapes, and that the “shape function / class function” methodology can be used to describe the fundamental shapes as well as the distributions of the fundamental shapes. A number of applications of the “CST” method to nacelles, ducts, wings and bodies were presented to illustrate the versatility of this new methodology. In this paper, the CST method is extended to include geometric warping such as variable camber, simple flap, aeroelastic and flutter deflections. The use of the CST method for geometric morphing of one geometry to another is also shown. The use of CST analytic wings in design optimization will also be discussed.

I. Introduction

The choice of the mathematical representations of the geometry of an aircraft or aircraft component, that is utilized in any particular aerodynamic design or multidisciplinary design optimization process, along with the selection of the type of optimization algorithm have a profound effect on such things as the computational time and resources, the extent and general nature of the design space which determines whether or not the geometries contained in the design space are smooth or irregular, or even physically realistic or acceptable.

The method of geometry representation also affects the suitability of the selected optimization process. For example the use of discrete coordinates as design variables may not be suitable for use with a genetic optimization process since the resulting design space could be heavily populated with airfoils having bumpy irregular surfaces, thus making the possibility of locating an optimum smooth practically impossible. The geometry representation method may also affect whether a meaningful “optimum” is contained in the design space and if an optimum design exists, whether or not it can be found.

Desirable characteristics for any geometric representation technique include:

- Well behaved and produces smooth and realistic shapes
- Mathematically efficient and numerically stable process that is fast, accurate and consistent
- Requires relatively few variables to represent a large enough design space to contain optimum aerodynamic shapes for a variety of design conditions and constraints
- Allows specification of design parameters such as leading edge radius, boat-tail angle, airfoil closure.
- Provides easy control for designing and editing the shape of a curve
- Intuitive - Geometry algorithm should have an intuitive and geometric interpretation.

The geometric definition of any aircraft consists of representing the basic defining components of the configuration by utilizing two fundamental types of shapes³ together with the distribution of the shapes along each of the components.

* Engineer/Scientist – Technical Fellow, Enabling Technology & Research, PO Box 3707, Seattle, WA 98124 / MS 67-LF, AIAA Member

The two fundamental defining shapes include:

Class 1: Wing airfoil type shapes for defining such components as:

- Airfoils / Wings
- Helicopter rotors, Turbomachinery blades
- Horizontal and Vertical tails, Canards, Winglets, Struts
- Bodies or Nacelles of revolution

Class 2: Body cross-section type shapes for defining such components as:

- Aircraft fuselages (cross sections)
- Rotor hubs and shrouds
- Channels, Ducts and tubing
- Lifting Bodies

The mathematical description of a class 1 geometries having a round nose and pointed aft-end is a continuous but non-analytic function because of the infinite slope at the nose and the corresponding large variations of curvature over the surface. Similarly, in the conventional Cartesian coordinate system, the mathematical definitions of the cross-sections of a class 2 type of geometries generally are also continuous but non-analytic functions.

Consequently, a large number of coordinates are typically required to describe either Class 1 or Class 2 types of geometries. Numerous methods^{4, 5, 6, 7, 8, 9, 10} have been devised to numerically represent class 1 airfoil type geometries for use in aerodynamic design, optimization and parametric studies. Commonly used geometry representation methods typically fail to meet the complete set of the previously defined desirable features¹.

A previous paper¹ focused on the class 1 type of 2D airfoil shapes that have a round nose and a pointed aft-end. A new and powerful methodology for describing such geometries was presented. In a subsequent paper², the methodology was extended to represent class II geometries as well as to general 3D geometries. In the current paper results of the extension of the CST method to more general wing / body geometries will be presented along with initial aerodynamic optimization results using the CST methodology.

A brief description and review of the methodology presented in the previous papers will be shown since knowledge of this information is essential to the understanding of the extension of the methodology that is presented in the present paper.

The concept of representing arbitrary 3D geometries as distribution of fundamental shapes is discussed. It is shown that the previously method developed for 2D airfoils and axi-symmetric bodies or nacelles, can be used to mathematically describe both the fundamental shapes as well as the distribution of the shapes for rather arbitrary 3D geometries. Applications of the extended methodology to a variety of 3D geometries including wings and nacelles are shown.

II. Round Nose Airfoil Representation

A typical subsonic wing airfoil section is shown in figure 1. Round nose airfoils such as shown in the figure, have an infinite slope and an infinite 2nd derivative at the leading edge and large variations in curvature over the airfoil surface. The mathematical description of an airfoil must therefore deal with a rather complex non-analytic function over the surface of the airfoil. Consequently a large number of “x,z” coordinates are typically required along with a careful choice of interpolation techniques in order to provide a mathematical or numerical description of the surfaces of an airfoil.

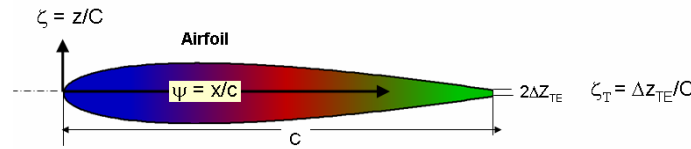


Figure 1: Typical Wing Airfoil Section

The choice of the mathematical representation of an airfoil, that is utilized in any particular aerodynamic design optimization process, along with the selection of the type of optimization algorithm have a profound effect on such things as:

- Computational time and resources
- The extent and general nature of the design space that determines whether or not the geometries contained in the design space are smooth or irregular, or even physically realistic or acceptable
- If a meaningful “optimum” is even contained in the design space
- If optimum designs exist, whether or not they can they be found.

The method of geometry representation also affects the suitability of the selected optimization process. For example the use of discrete coordinates as design variables may not be suitable for use with a genetic optimization process since the resulting design space could be heavily populated with airfoils having bumpy irregular surfaces, thus making the possibility of locating an optimum smooth practically impossible.

Desirable design features for any geometric representation technique include:

- Well behaved and produces smooth and realistic shapes
- Mathematically efficient and numerically stable process that is fast, accurate and consistent
- Flexibility
 - Requires relatively few variables to represent a large enough design space to contain optimum aerodynamic shapes for a variety of design conditions and constraints
 - Allows specification of key design parameters such as leading edge radius, boat-tail angle, airfoil closure.
 - Provide easy control for designing and editing the shape of a curve
- Intuitive - Geometry algorithm should have an intuitive and geometric interpretation.
- Systematic and Consistent - The way of representing, creating and editing different types of curves (*e.g.*, lines, conic sections and cubic curves) must be the same.
- Robust - The represented curve will not change its geometry under geometric transformations such as translation, rotation and affine transformations.

Commonly used geometry representation methods typically fail to meet the complete set of desirable features¹.

III. Mathematical Description of Airfoil Geometry

In the case of the round nose airfoil described in a fixed Cartesian coordinate system, the slopes and 2nd derivatives of the surface geometry are infinite at the nose and large changes in curvature occur over the entire airfoil surface. The mathematical characteristics of the airfoil surfaces are therefore non-analytic function with singularities in all derivatives at the nose. The approach used in reference 1 to develop an improved airfoil geometry representation method is based on a technique that the author has often used successfully in the past, to develop effective computational methods to deal with numerically difficult functions.

The technique included the following steps:

1. Develop a general mathematical equation necessary and sufficient to describe the geometry of any round nose / sharp aft end airfoil;
2. Examine the general nature of this mathematical expression to determine the elements of the mathematical expression that are the source of the numerical singularity
3. Rearrange or transform the elements of the mathematical expression to eliminate the numerical singularity.
4. This resulted in identifying and defining a “shape function” transformation technique such that the “design space” of an airfoil utilizing this shape function becomes a simple well behaved analytic function with easily controlled key physical design features in addition to possessing an inherent strong smoothing capability.
5. Subsequently a “Class Function” was introduced to generalize the methodology for applications to a wide variety of fundamental 2D airfoils and axi-symmetric nacelle and body geometries.

A summary of this approach is discussed below.

The general and necessary form of the mathematical expression that represents the typical airfoil geometry shown in figure 1 is:

$$\zeta(\psi) = \sqrt{\psi}(1-\psi) \sum_{i=0}^N A_i \psi^i + \psi \zeta_T \quad (1)$$

Where: $\psi = x/c$ $\zeta = z/c$ and $\zeta_T = \Delta \zeta_{TE}/c$.

The term $\sqrt{\psi}$ is the only mathematical function that will provide a round nose.

The term $(1-\psi)$ is required to insure a sharp trailing edge.

The term $\psi \zeta_T$ provides control of the trailing edge thickness.

The term $\sum_{i=0}^{\infty} A_i \psi^i$ represents a general function that describes the unique shape of the geometry between the round nose and the sharp aft end. This term is shown for convenience as a power series but it can be represented by any appropriate well behaved analytic mathematical function.

IV. Airfoil Shape Function

The source of the non-analytic characteristic of the basic airfoil equation is associated with the square root term in equation 1.

Let us define the shape function “S(ψ)” that is derived from the basic geometry equation by first subtracting the base area term and then dividing by the round nose and sharp end terms.

This gives:

$$S(\psi) \equiv \frac{\zeta(\psi) - \psi \zeta_T}{\sqrt{\psi} \bullet [1-\psi]} \quad (2)$$

The equation that represents the “S” function which is obtained from equations 1 and 2 becomes the rather simple expression:

$$S\left(\frac{x}{L}\right) = \sum_{i=0}^N \left[A_i \bullet \left[\frac{x}{L} \right]^i \right] \quad (3)$$

The “shape function” equation is a simple well behaved analytic equation for which the “eye” is well adopted to see the represented detailed features of an airfoil and to make critical comparisons between various geometries.

It was shown in reference 1, that the nose radius, the trailing edge thickness and the boat-tail angle are directly related to the unique bounding values of the “S(ψ)” function.

The value of the shape function at $x/c = 0$ is directly related to the airfoil leading edge nose radius by the relation:

$$S(0) = \sqrt{2 R_{LE} / C} \quad (4)$$

The value of the shape function at $x/c = 1$ is directly related to the airfoil boat-tail angle, β , and trailing edge thickness, ΔZ_{te} , by the relation:

$$S(1) = \tan \beta + \frac{\Delta Z_{te}}{C} \quad (5)$$

Hence, in the transformed coordinate system, specifying the endpoints of the “S” function provide and an easy way to define and to control the leading edge radius, the closure boat-tail angle and trailing edge thickness.

An example of the transformation of the actual airfoil geometry to the corresponding shape function is shown in figure 2. The transformation of the constant Z_{MAX} height line, and the constant boat-tail angle line, are also shown in the transformed plane.

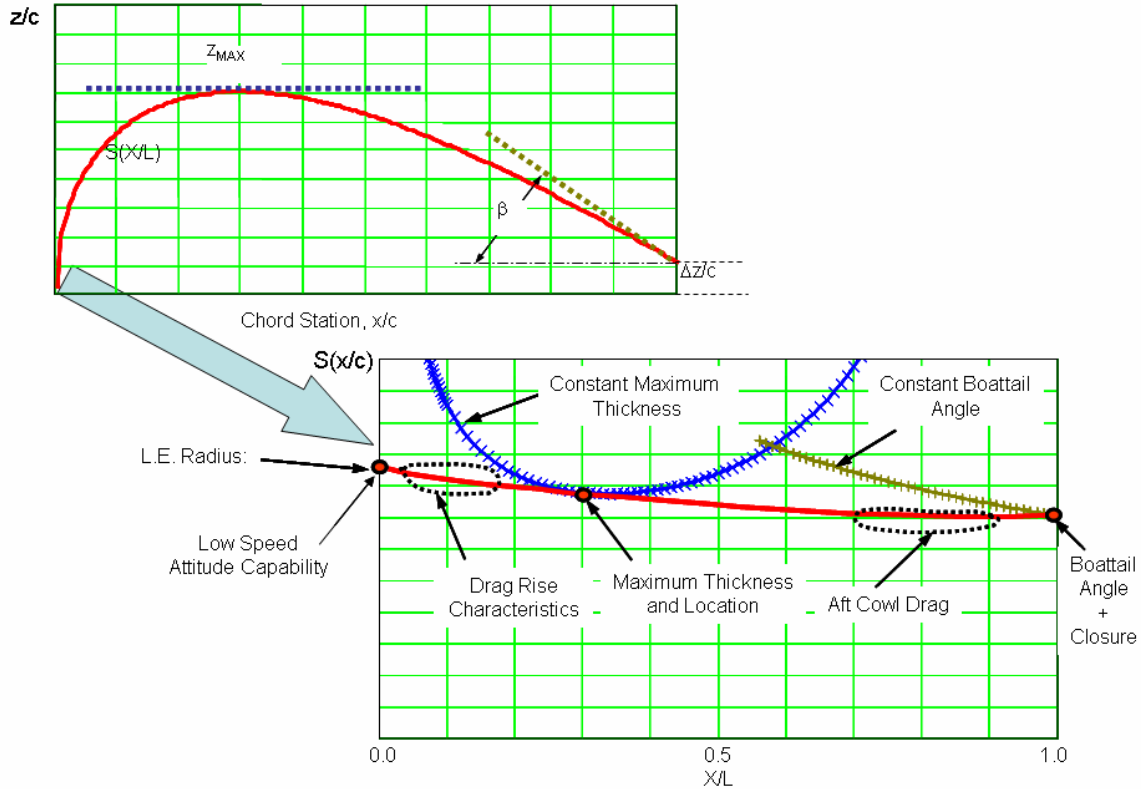


Figure 2: Example of an Airfoil Geometric Transformation

The shape function for this example airfoil is seen to be approximately a straight line with the value at zero related to the leading edge radius of curvature and the value at the aft end equal to tangent of the boat-tail angle plus the ratio of trailing edge thickness / chord length. It is readily apparent that the shape function is indeed a very simple analytic function.

The areas of the airfoil that affects its drag and performance characteristics of the airfoil are readily visible on the shape function curve as shown in the figure. Furthermore, the shape function provides easy control of the airfoil critical design parameters.

The term $\sqrt{\psi} [1 - \psi]$ will be called the “Class Function” $C(\psi)$ With the general form

$$C_{N2}^{N1}(\psi) = (\psi)^{N1} [1 - \psi]^{N2} \quad (6)$$

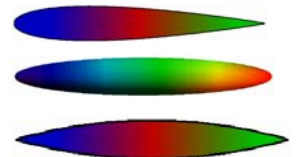
For a round nose airfoil $N1 = 0.5$ and $N2 = 1.0$

In reference 1, it was shown that different combinations of the exponents in the class function define a variety of basic general classes of geometric shapes:

$N1 = 0.5$ and $N2 = 1.0$ define a NACA type round nose and pointed aft end airfoil.

$N1 = 0.5$ and $N2 = 0.5$ define an elliptic airfoil, or an ellipsoid

$N1 = 1.0$ and $N2 = 1.0$ define a biconvex airfoil, or an ogive body.

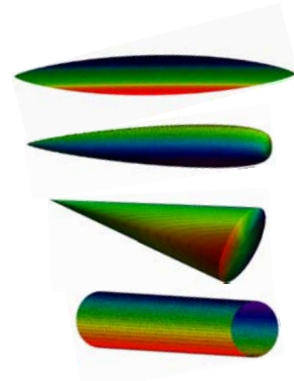


$N1 = 0.75$ and $N2 = 0.75$ define the radius distribution of a Sears-Haack body

$N1 = 0.75$ and $N2 = 0.25$ define a low drag projectile

$N1 = 1.0$ and $N2 = 0.001$ define a cone or wedge airfoil.

$N1 = 0.001$ and $N2 = 0.001$ define a rectangle, or circular rod.



The “class function” is used to define general classes of geometries, where as the “shape function” is used to define specific shapes within the geometry class.

Defining an airfoil shape function and specifying it’s class function is equivalent to defining the actual airfoil coordinates which are obtained from the shape function and class function as:

$$\zeta(\psi) = C_{N2}^{N1}(\psi) \cdot S(\psi) + \psi \cdot \zeta_T \quad (7)$$

V. Representing the Shape Function

A number of different techniques of techniques of representing the shape function for describing various geometries will be described in this report. The simplest approach is illustrated in Figure 3. The figure shows the fundamental baseline airfoil geometry derived from the simplest of all shape functions, the unit shape function: $S(\psi) = 1$. Simple variations of the baseline airfoil are also shown with individual parametric changes of the leading edge radius, and of the location of maximum thickness.

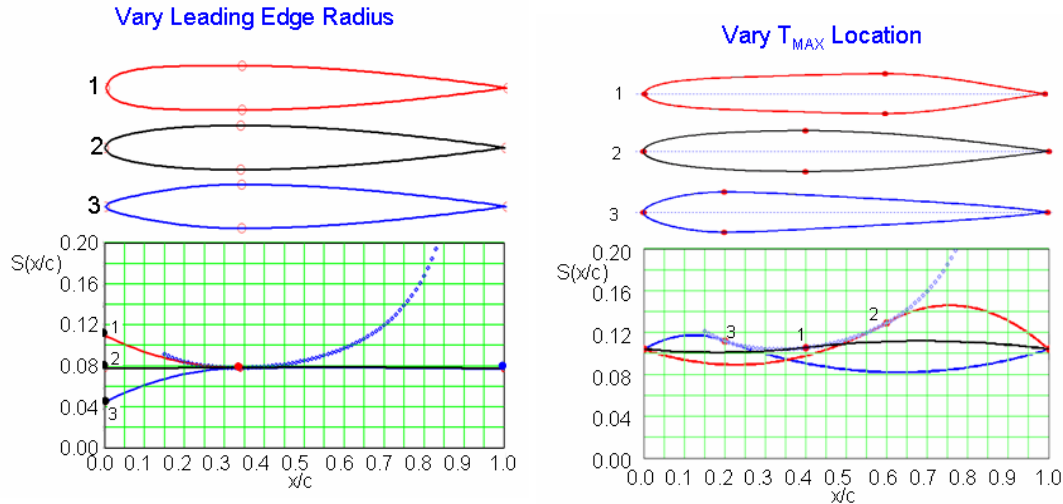


Figure 3: Examples of One Variable Airfoil Variations

The figure on the left shows changes in the leading edge radius and the front portion of the airfoil obtained by varying the value of $S(0)$ with a quadratic equation that is tangent to the Z_{max} curve at x/c for Z_{max} . The maximum thickness, maximum thickness location and boat-tail angle remained constant.

The figure on the right shows variations in boat-tail angle obtained by changing the value of the shape factor at the aft end, $x/c = 1$ while the front of the airfoil is unchanged. In each of these examples the airfoil shape changes are controlled by a single variable and in all cases the resulting airfoil is both smooth and continuous

Figure 4 shows a five variable definition of a symmetric $C_{1.0}^{0.5}(\psi)$ airfoil using the shape function. The corresponding airfoil geometry is also shown. The variables include:

1. Leading edge radius
2. Maximum thickness
3. Location of maximum thickness
4. Boattail Angle
5. Closure Thickness

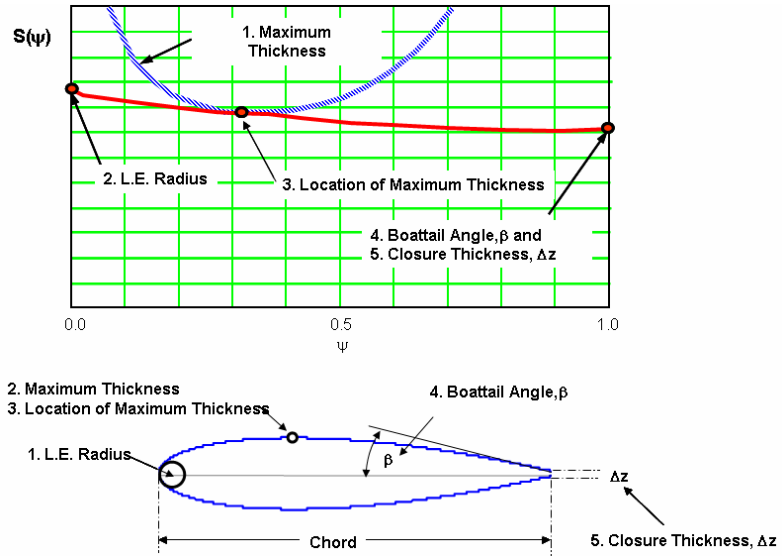


Figure 4: Symmetric Airfoil Five Variables Definition

A cambered airfoil can be defined by applying the same technique to both the upper and the lower surfaces. In this instance the magnitude of the value of the shape function at the nose, $S(0)$, of the upper surface is equal to that on the lower surface. This insures that the leading edge radius is continuous from the upper to the lower surface of the airfoil. The value of the half thickness at the trailing edge is also equal for both surfaces. Consequently, as shown in figure 5, eight variables would be required to define the aforementioned set of parameters for a cambered airfoil.

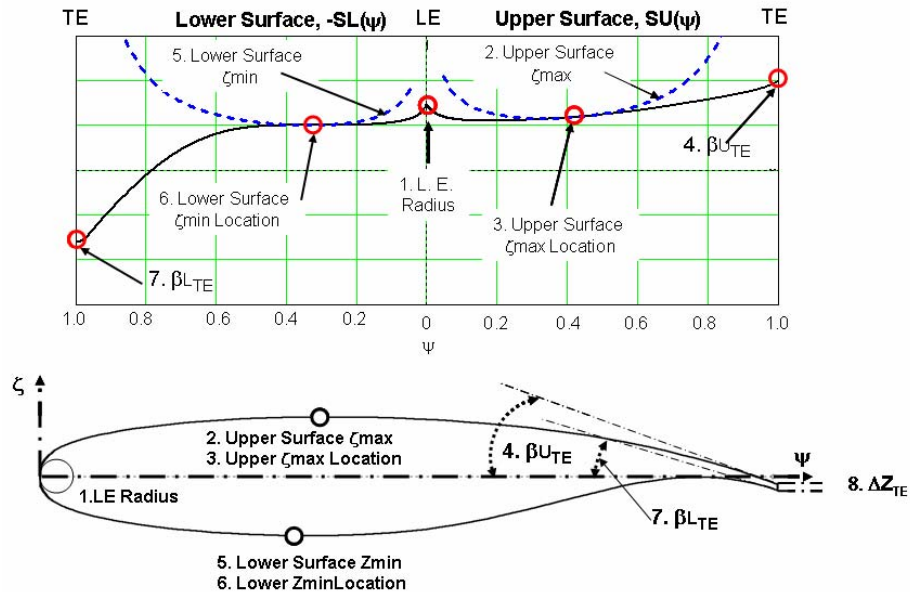


Figure 5: Cambered Airfoil Eight Variables Definition

In the examples shown in figure 4 and figure 5, the key defining parameters for the airfoils are all easily controllable with the shape function.

VI. Airfoil Decomposition into Component Shapes

The unit shape function can be decomposed into scalable component airfoils¹ by representing the shape function with a Bernstein polynomial of order “N” as shown in figure 6.

The representation of the unit shape function in terms of increasing orders of the Bernstein polynomials provides a systematic decomposition of the unit shape function into scaleable components. This is the direct result of the “Partition of Unity” property which states that the sum of the terms, which make up a Bernstein polynomial of any order, over the interval of 0 to 1, is equal to one. This means that every Bernstein polynomial represents the unit shape function. Consequently, the individual terms in the polynomial can be scaled to define an extensive variety of airfoil geometries¹.

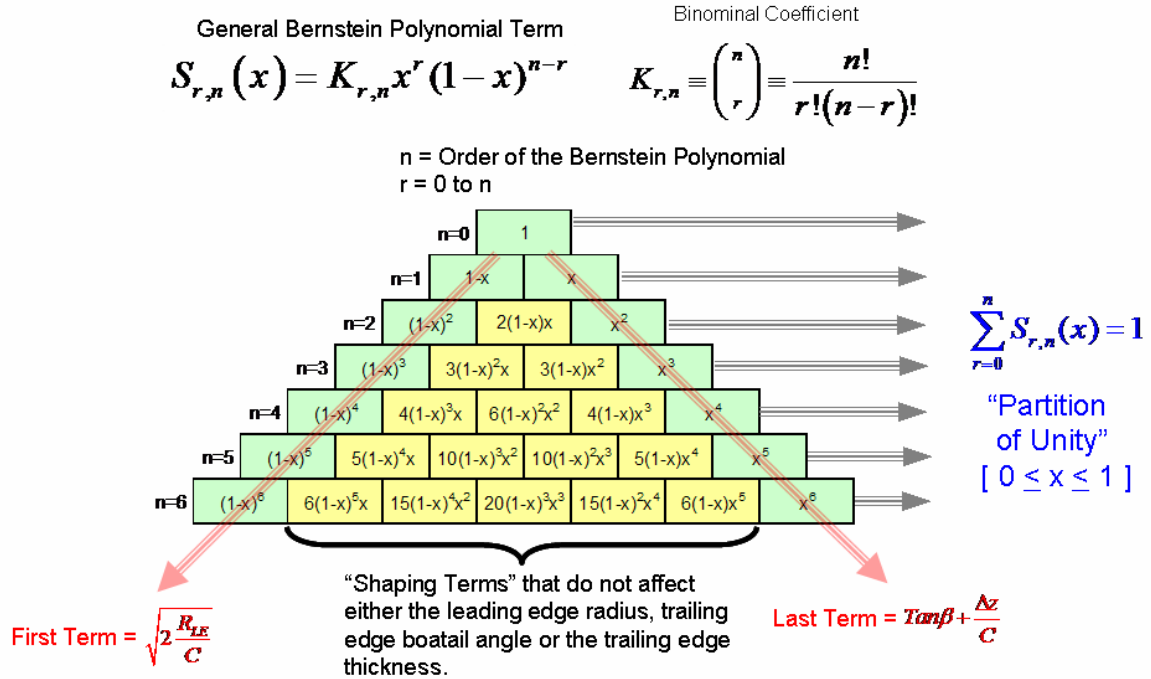


Figure 6: Bernstein Polynomial Decomposition of the Unit Shape Function

The Bernstein polynomial of any order “n” is composed of the “n+1” terms of the form:

$$S_{r,n}(x) = K_{r,n} x^r (1-x)^{n-r} \quad (8)$$

r = 0 to n

n = order of the Bernstein polynomial

In the above equation, the coefficients factors $K_{r,n}$ are binominal coefficients defined as:

$$K_{r,n} = \binom{n}{r} = \frac{n!}{r!(n-r)!} \quad (9)$$

For any order of Bernstein polynomial selected to represent the unit shape function, only the first term defines the leading edge radius and only the last term defines the boat-tail angle. The other in-between terms are “shaping terms” that neither affect the leading edge radius nor the trailing edge boat-tail angle.

Examples of decompositions of the unit shape function using various orders of Bernstein polynomials are shown in figure 7 along with the corresponding component airfoils.

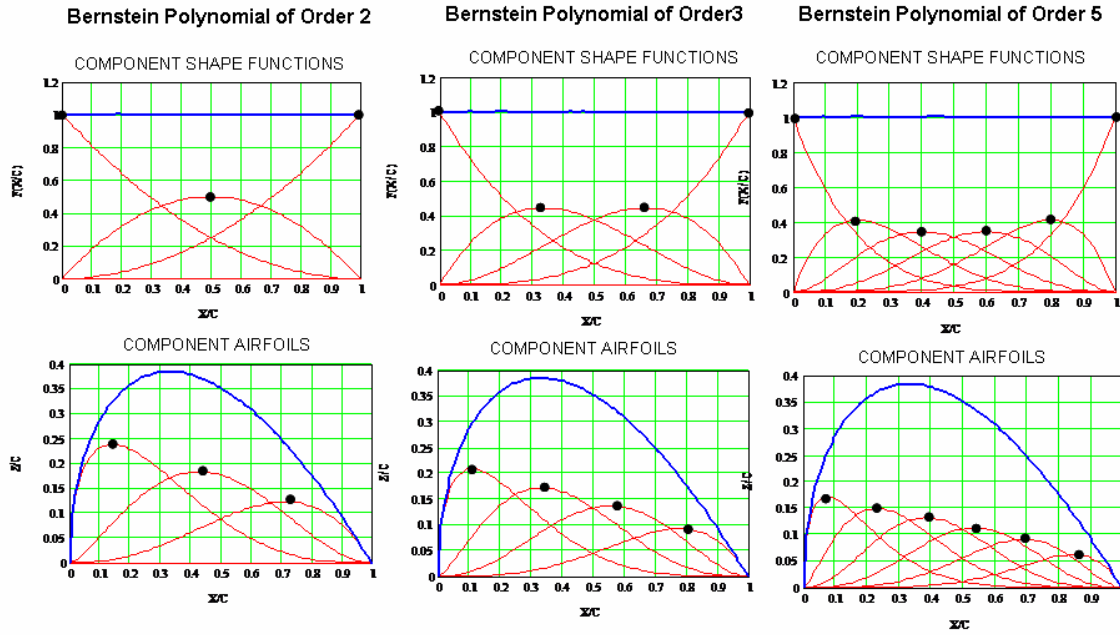


Figure 7: Bernstein Polynomial Provides “Natural Shapes”

The locations of the peaks of the component “S” functions are equally spaced along the chord as defined by the equation:

$$(\psi)_{S_{\max i}} = \frac{i}{n} \quad \text{for } i = 0 \text{ to } n \quad (10)$$

The corresponding locations of the peaks of the component airfoils are also equally spaced along the chord of the airfoil and are defined in terms of the class function exponents and the order of the Bernstein polynomial by the equation:

$$(\psi)_{Z_{\max}} = \frac{N1+i}{N1+N2+n} \quad \text{for } i = 0 \text{ to } n \quad (11)$$

The technique of using Bernstein polynomials to represent the shape function of an airfoil in reality defines a systematic set of component airfoil shapes that can be scaled to represent a variety of airfoil geometries as shown in figure 8.

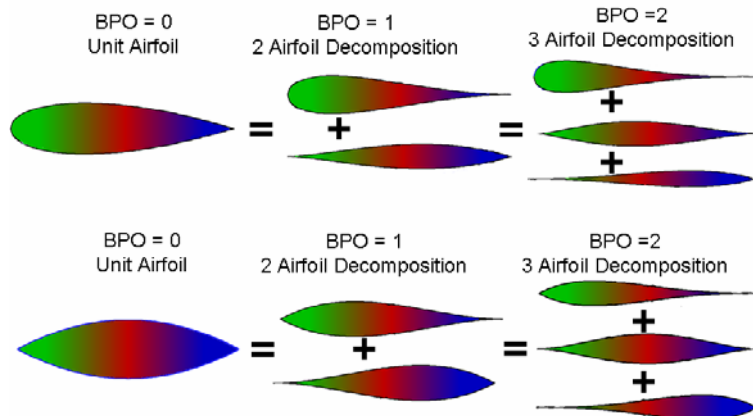


Figure 8: Example Component Airfoils

VII. Airfoils Defined Using Bernstein Polynomials Representation of the Unit Shape Function

The upper and lower surfaces of a cambered airfoil, can each be defined using Bernstein Polynomials of any selected order n , to describe a set of component shape functions that are scaled by “to be determined” coefficients as shown in the following equations.

The component shape functions are defined as: $S_i(\psi) = K_i \psi^i (1-\psi)^{n-i}$ (12)

Where the term K_i is the binomial coefficient which is defined as: $K_i \equiv \binom{n}{i} = \frac{n!}{i!(n-i)!}$ (13)

Let the trailing edge thickness ratios for the upper and lower surface of an airfoil be defined as:

$$\Delta \xi_U = \frac{z_{TE}}{C} \quad \text{and} \quad \Delta \xi_L = \frac{z_{TE}}{C} \quad (14)$$

The class function for the airfoil is: $C_{N2}^{N1}(\psi) = \psi^{N1} \bullet (1-\psi)^{N2}$ (15)

The overall shape function equation for the upper surface is: $S_u(\psi) = \sum_{i=1}^n A u_i \bullet S_i(\psi)$ (16)

The upper surface defining equation is: $(\zeta)_{Upper} = C_{N2}^{N1}(\psi) \bullet S_l(\psi) + \psi \bullet \Delta \xi_{Upper}$ (17)

The lower surface is similarly defined by the equations: $S_l(\psi) = \sum_{i=1}^n A l_i \bullet S_i(\psi)$ (18)

and $(\zeta)_{Lower} = C_{N2}^{N1}(\psi) \bullet S_l(\psi) + \psi \bullet \Delta \xi_{Lower}$ (19)

The coefficients $A u_i$ and $A l_i$ can be determined by a variety of techniques depending on the objective of the particular study. Some examples include:

- Variables in a numerical design optimization application
- Least squares fit to match a specified geometry
- Parametric shape variations.

The method of utilizing Bernstein polynomials to represent an airfoil has the following unique and very powerful properties¹:

- This airfoil representation technique, captures the entire design space of smooth airfoils
- Every airfoil in the entire design space can be derived from the unit shape function airfoil
- Every airfoil in the design space is therefore derivable from every other airfoil

IV. Airfoil Representation → Key Convergence Question

A key convergence question relative to the class function / shape function geometry method for defining airfoils, nacelles or bodies of revolution is the following. What orders of Bernstein polynomials, BPO, are required to capture enough of a meaningful design space to contain a true optimum design?

A two step approach was defined in order to obtain the answer for this question:

- 1) Compare actual airfoil and represented airfoil geometries for a wide variety of airfoils
 - Use various orders of Bernstein polynomials for the shape function to approximate the actual airfoils shape functions computed from the defined airfoil coordinates. The coefficients for the component Bernstein polynomial shape functions were to be determined by least squares fits to the selected airfoil upper and lower surface shape functions. For all study airfoils, approximate airfoils were determined for Bernstein polynomial representation of the shape functions of orders 2 to 15/
 - Investigate a wide variety of optimum and non-optimum, symmetric and cambered airfoil geometries.
 - Compute the statistical measures such as “residual differences”, “standard deviations” and “correlation functions” to quantify the “mathematical goodness” of the representations for each of the study airfoils.
 - Compare surface slopes, 2nd derivatives and curvature between actual and approximate airfoil shapes
- 2) Conduct TRANAIR^{11,12} with boundary layer CFD analyses of the actual and the corresponding shape function defined airfoils for a range of Mach numbers and angle of attacks.
 - Compare upper and lower surface pressure distributions between those obtained with the actual and approximate geometries.
 - Compare lift, drag and pitching moment characteristics between the actual and approximate airfoils

More than 30 airfoils have been analyzed applying this process. These include symmetric NACA airfoils, cambered NACA airfoils, high lift airfoils, natural laminar flow airfoils, shock-free airfoils, supercritical airfoils and transonic multipoint optimized airfoils. For each of the study airfoils, approximate airfoil geometries were defined using Bernstein polynomial surface representations of the upper and lower surfaces shape functions, of orders 2 to 15, to critically evaluate the geometry convergence characteristics. Results of these extensive investigations were reported in reference 1.

Typical examples of shape function representation of a variety of airfoils is shown in figure 9. The defining airfoil coordinates are shown by the circles. The approximating geometries are shown as the lines through the points. Bands corresponding to typical wind tunnel tolerances are shown in the coordinate residual curves. Bars corresponding to ½ of the height of the circular symbols representing the actual airfoil geometry, are indicated on the figures.

The results of the previously reported extensive¹ assessments of the adequacy of the shape function methodology utilizing Bernstein polynomials to represent a wide variety of airfoils, showed that a relatively low order Bernstein polynomial, (typically BPO6 to BPO9), matched the airfoils geometries, slopes and 2nd derivatives as well as the pressure distributions and aerodynamic forces¹. The results also indicated that lower order Bernstein polynomials, corresponding to fewer design variables, (perhaps BPO4 to BPO6), should be adequate for developing optimum designs.

The CST methodology offers the option for a systematic approach for design optimization. The optimization process can initially be conducted with a family of component airfoil shapes corresponding to a low order BP representation for the shape function to obtain an optimum design. The order of the BP can then be increased to conduct another optimization to determine if a better optimum design is achieved. Increasing the order of the BP is a systematic way to increase the number of design variables and thereby explore the convergence to an optimum solution.

Figure 10 shows examples of geometric warping. These were obtained by defining the forward and aft pivot points. The chord lines forward of the front pivot point and aft of the back pivot point are deflected according to a prescribed deflection shape. The simple flap has a discontinuous linear rotation. The variable camber is obtained with a cubic equation. Both type of deflections have two variables that include the pivot point location and the shape exponent of the deflection curve. The physical length of the deflected chord is retained. The original upper and lower surface local heights normal to the chord length are retained along the deflected chords.

The aeroelastic deflections were obtained in a similar manner.

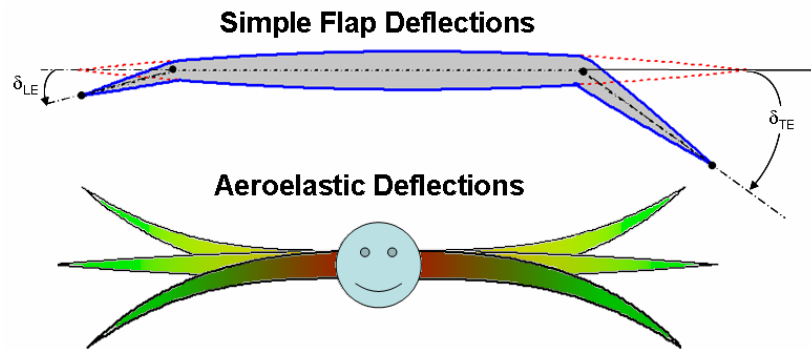


Figure 10: Examples of Geometric Warping

The discussions so far have been focused in 2D round nose / sharp aft-end airfoils. However, as shown in figure 11, different combinations of the exponents in the class function defines a variety of basic general classes of geometric shapes of airfoils, bodies of revolution and axi-symmetric nacelles. The use of the class function therefore, allows the previously discussed shape function methodology as well as the studies conclusions to apply equally well to a wide variety of 2D and axi-symmetric geometries.

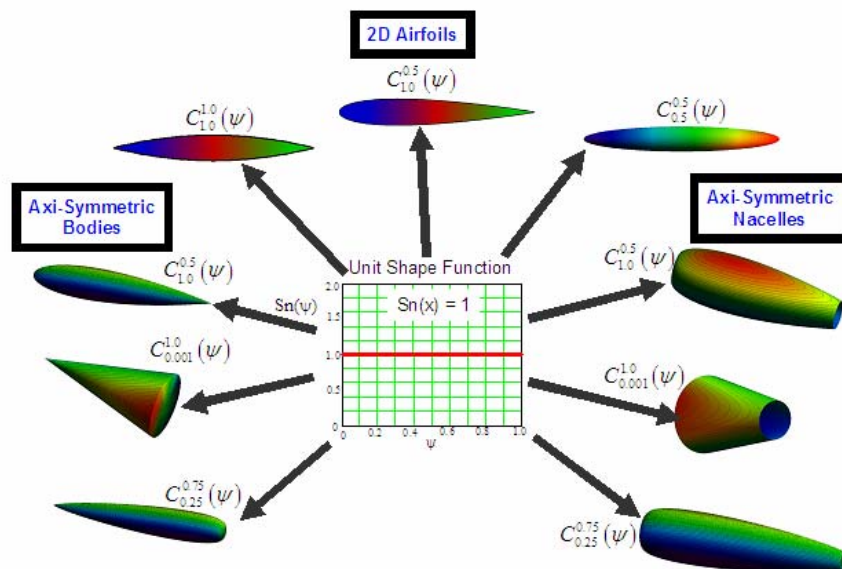


Figure 11: Geometries Derivable From a Unit Shape Function

IX. Extension to Arbitrary 3D Geometries

The shape functions / class function methodology can be used to describe both the upper and the lower lobes of a body cross section similar to the upper and lower surface of an airfoil. Let us initially assume that a body cross-section is laterally symmetric and has the shape of an ellipse as shown in the figure 12. We will then subsequently generalize the results using the class function.

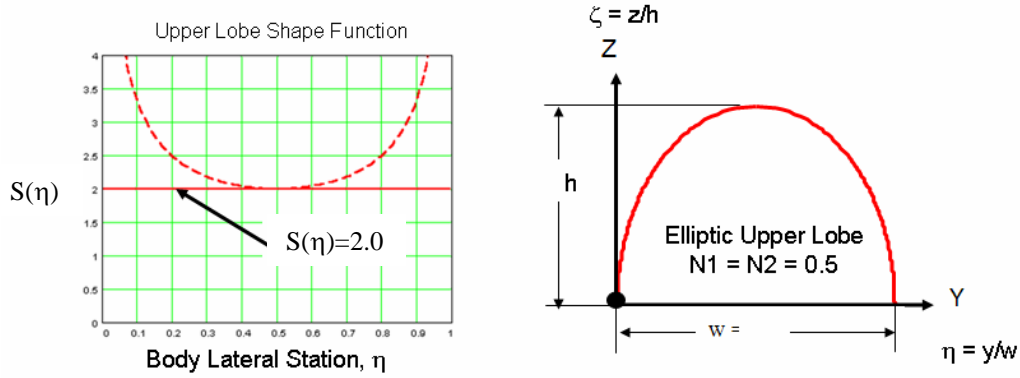


Figure 12: Representation of a Body Upper or Lower Lobe Shape

The equation for the ellipse with the axes of the ellipse at the left edge can be expressed as:

$$\zeta(\eta) = 2\eta^{0.5}(1-\eta)^{0.5} \quad (20)$$

Where: $\eta = y/w$ and $\zeta = z/h$

The shape function for this upper lobe elliptic geometry is therefore:

$$Su(\eta) = \frac{\zeta u(\eta)}{\eta^{NC1}(1-\eta)^{NC2}} = 2 \quad (21)$$

In the above equation we have generalized the expression by using the arbitrary exponents NC1 and NC2

$$Cs(\eta) = \eta^{NC1}(1-\eta)^{NC2} \quad (22)$$

$Cs(\eta)$ will be called the cross-section class function.

In this case the upper lobe defining equation is: $\zeta u(\eta) = [Su(\eta) \equiv 2] Cs_{0.5}^{0.5}(\eta)$ (23)

For an elliptic upper lobe shape, the shape function is a constant and equal to 2.0, and the class function exponents are: $NC1 = NC2 = 0.5$

Figure 13 shows examples of variety of cross section shapes that can be obtained by independently varying the class function coefficients for the upper and lower lobes of the body cross section. In these examples, the shape function is a constant value. Any of the geometries can be morphed from the circle by continuously varying the class function coefficients from those of the circle to those of the desired geometric shape. The condition of constant cross sectional area during the geometric morphing can be easily imposed.

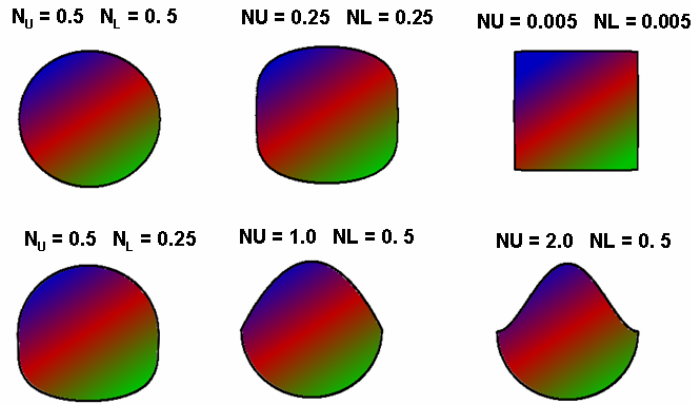


Figure 13: Example Upper Lobe / Lower Lobe Body Cross sections

By using the previously described Bernstein polynomial technique to represent the unit shape function together with the body cross-section aspect ratio of the body cross-section (ratio of body cross-section width to body cross-section height), a limitless variety of smooth cross-sectional geometries can be generated with just a few variables.

The example cross-sections shown in figures 13 were obtained using simple unit shape functions but different class functions. Very general cross-sectional shapes can be generated by varying the shape function formulations in addition to the class functions. As shown in figure 14, changing the shape function for the upper body lobe can create upper surface bumps or fairings. In the examples shown, the geometries are representative of a cross-section of a fuselage through the cockpit area.

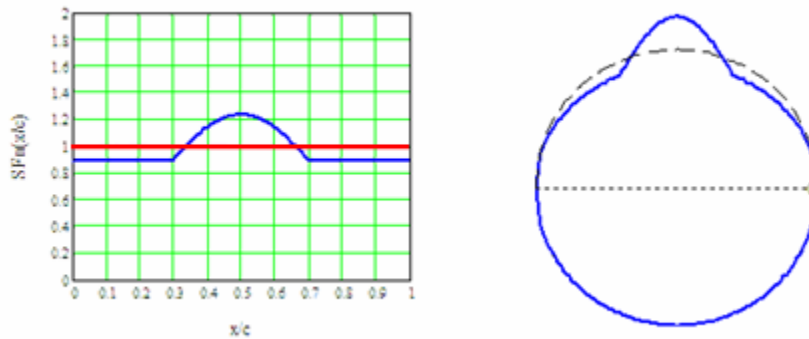


Figure 14: Fuselage “Bump” Representation

Three dimensional bodies in general can be represented as a cross-sectional shape together with a distribution or morphing of the cross-section shape along the length of the body. This is shown in figure 15 by the examples of a duct, a high aspect ratio wing, and a supersonic type integrated wing body.

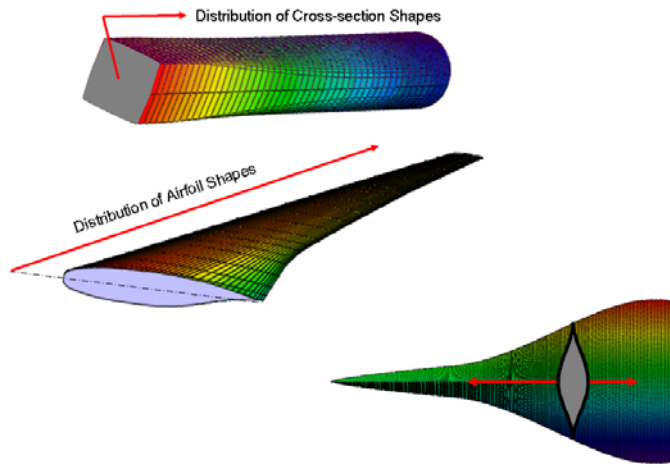


Figure 15: Examples of 3D Geometries as Distribution of Shapes

The concept of using the shape function / class function methodology to describe both the fundamental cross-sectional shapes and the distribution of the shapes along the body axis is shown for the simple case of a cube in figure 16.

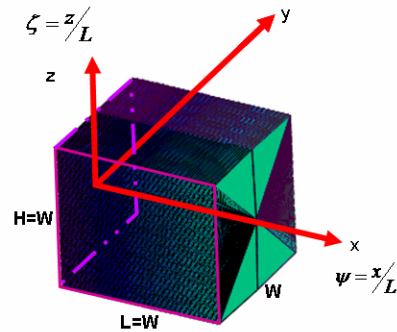


Figure 16: Definitions of Cross-Section Shape and Distribution

The square cross-section can be described by a class function with “zero exponents”, $Cs_{0.005}^{0.005}(\eta)$, and a unit shape function. The longitudinal area distribution controls the distribution of the cross section shapes. The longitudinal area distribution for a cube can be represented by a similar class function, $Cd_{0.005}^{0.005}(\psi)$.

Figure 17 shows a number of relatively simple 3D bodies that can be obtained by various combinations of the cross section and distribution class function exponents. Comparing the third and fourth geometries in the figure, it can be seen that a distribution class function exponent slightly greater than zero results in a solid geometry while a distribution class function exactly equal to zero results in a similar but flow through geometry.

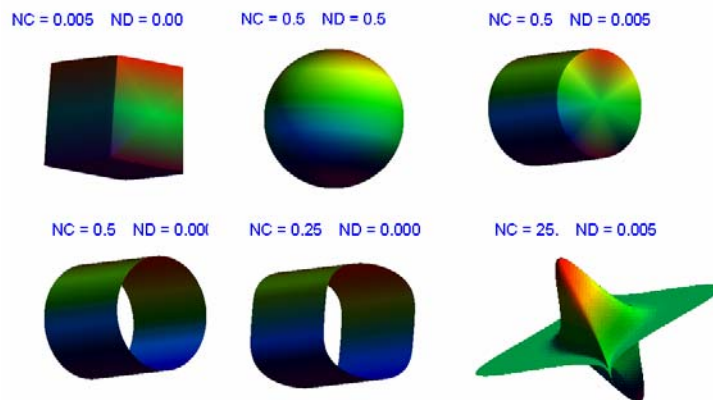


Figure 17: Simple 3D Bodies obtained by Various Cross Section and Distribution Class Function Exponents

Figure 18 shows an example of using the shape function / class function methodology to make an apparently significant geometry changes with very few design variables, by morphing a cube into an equal volume Sears-Haack body.

The circular cross-section of the Sears-Haack body has unit shape function and class functions exponents equal to $Cs_{0.5}^{0.5}(\eta)$. The longitudinal radius distribution of a Sears-Haack body has a unit shape function and a class function equal to $Cd_{0.75}^{0.75}(\psi)$.

Consequently the morphing of the cube into a Sears-Haack body is easily obtained by simultaneous:

- Increasing the cross-section class function exponents from 0.005 to 0.5
- Increasing the longitudinal radius distribution class function exponents from 0.005 to 0.75
- Increasing the length to keep the volume constant.

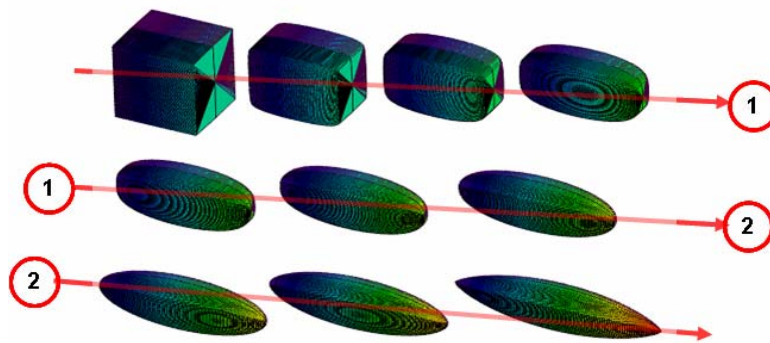


Figure 18: Three Variable Morphing of a Cube into a Sears-Haack Body

An example of morphing a constant area circular duct into a duct with geometry that varies from a circular inlet to a square shaped nozzle is shown in figure 19. This seemingly complicated geometric transformation was easily defined using as a single variable the class function exponents

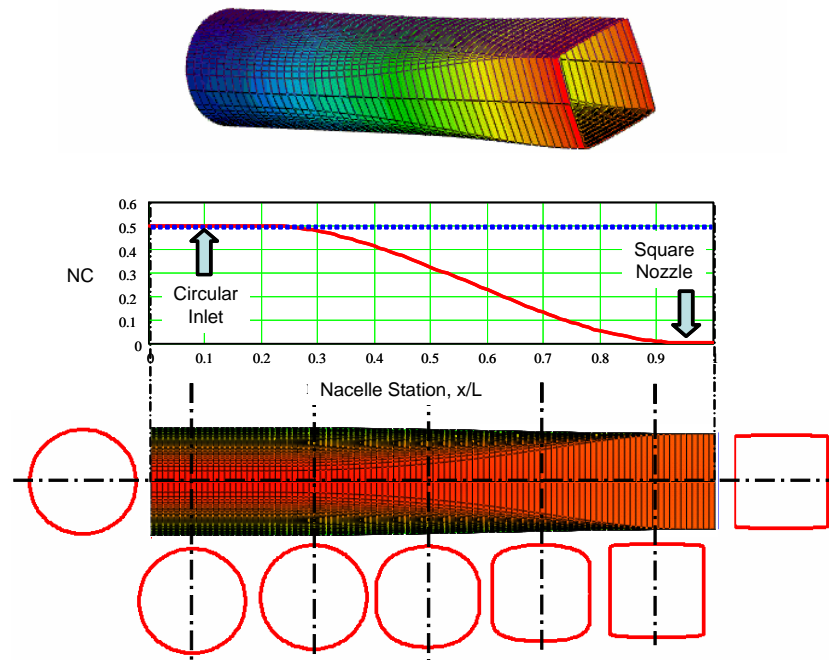


Figure 19: One Variable Definition of a Circular Duct With a Square Nozzle

The initial geometry shape at the inlet is a circular duct defined with a cross-section class function with exponents equal to “0.5”. The duct geometry, in this example, retains a constant cross section from 0 to 20% of the length. The last 5% length of the duct has a square cross-section which has class function exponents equal to “0.005”. The width/depth of the square were sized to match the circular inlet area.

In between 20% and 95% of the length, the class function exponents were decreased from 0.5 at 20% to 0.005 at 95% by a cubic variation with zero slopes at both ends. Along the transition region the width and depth were scaled proportionally to keep the cross section area constant. The entire geometry is in reality driven by a single variable, the aft end constant class function exponent

This is an example of a “scalar” or “analytic” loft in which the geometry is generated by the analytic variation of the shape defining parameters along the length of the duct.

By adding as an additional variable, the body cross section aspect ratio, the circular duct can be morphed into a duct having a circular inlet and transitions into a wide rectangular nozzle as shown in figure 20. The body cross section aspect ratio is defined as the ratio of body width to body height.

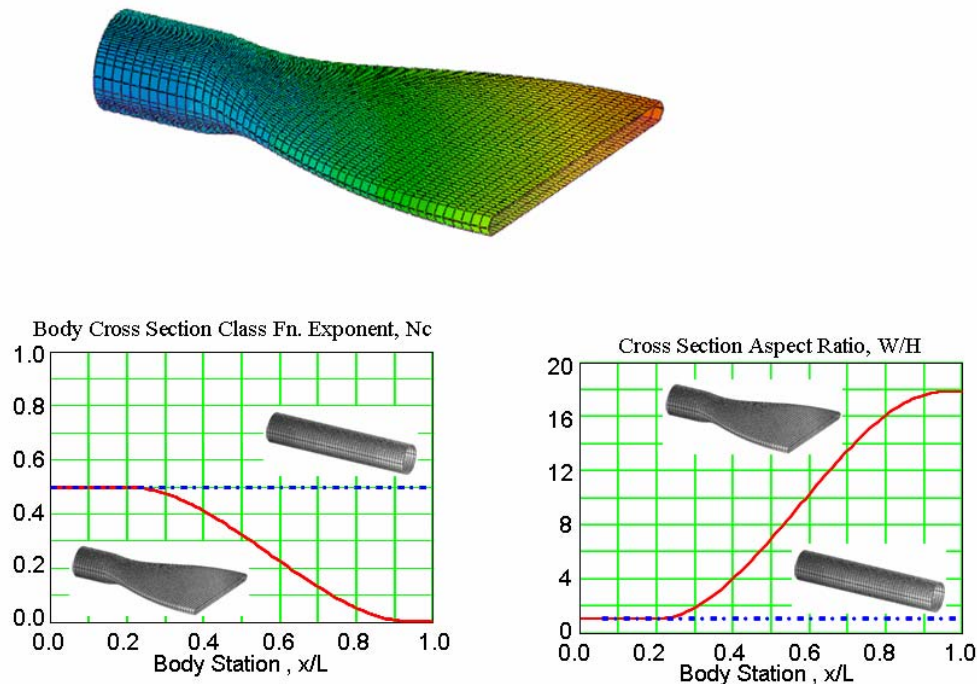


Figure 20: Two Variable Transformation of a Circular Duct to a Thin Rectangular Nozzle

In figure 21, using a similar technique to that used to define the duct in figures 19 and 20, a flow through circular duct is transformed a solid geometric shape that appears very similar to a supersonic aircraft configuration.

This geometric transformation was obtained with a total of four design variables. The four design variables included:

- Longitudinal class function exponents: Nd1, Nd2
- Aft end cross-section class function exponent, NC,
- the width to height ratio at the aft end: e2

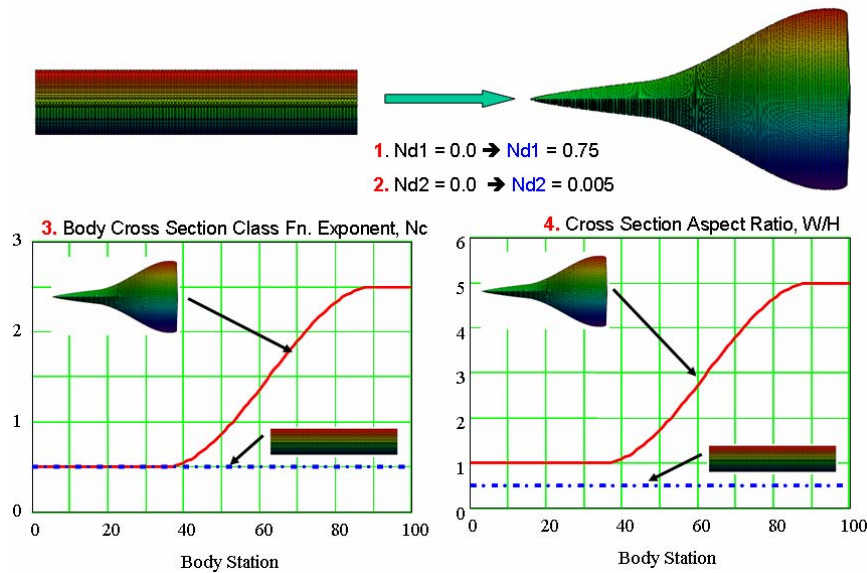


Figure 21: Transformation of a Circular Cylinder in a “Supersonic Transport”

X. Nacelle Design – 2 Options

There are two options for using class functions and shape functions for defining a nacelle. These include

1. Define Longitudinal profile shapes for crown line, maximum half-breadth, and keel line and then distributing these profiles circumferentially around the longitudinal axis to define the nacelle geometry
2. Define cross section shapes and distribute the shapes along the longitudinal axis as controlled by an area distribution.

In the discussions that follow, we will focus on the 1st option, since this will provide a demonstration of the combined use of many of the concepts that have been discussed in this report and in the previous studies^{1,2}. The objective is to develop a detailed nacelle definition with the use of very few design variables.

Figure 22 shows the common approach to defining a nacelle using airfoil type sections for the crown line, keel line and maximum half breadth shapes. In the example, the basic airfoil geometry is represented by a BP5 shape function definition for a supercritical type airfoil which therefore has 6 defining variables.

The keel line airfoil and the max half breadth airfoils in this example are both parametrically modified forward of the maximum thickness station to increase the leading edge radius in the former case and decrease the leading edge radius in the latter case. This results in the addition of two more defining variables corresponding to the desired leading edge radii.

The external cross-sectional shape of the nacelle between the crown, max half breadth and keel is defined by an upper lobe class function with the exponent NU. The lower lobe of the nacelle is similarly defined by lower lobe class function with the exponent NL. This approach to distribute the longitudinal airfoil shapes circumferentially around the nacelle is shown in figure 23. This is achieved by the use of cross section class functions in which the class function exponents are varied along the length of the nacelle as shown in the figure.

The upper lobe for the entire nacelle is defined using a constant class function exponents of 0.5. This results in an elliptic / circular cross sectional shape distribution between the crown line and the maximum half breadth airfoils.

The lower lobe cross-section class function exponents equal 0.25 out to defining station 1 which is located at 40% of the nacelle length. This results in a “squashed” shape distribution from the maximum half breadth airfoil to the keel line airfoil over the front portion of the nacelle.

The lower lobe aft of defining station 2, which occurs at 80% of the nacelle length, is circular with a class function exponent equal to 0.5. Consequently this results in an axi-symmetric nozzle geometry.

In between station 1 and station 2, the lower lobe shape joining the maximum half breath geometry and the keel geometry, varies smoothly from a squashed section at station 1 to a circular section at station 2.

The cross-sectional shape distribution is therefore defined entirely by the following 4 design variables:

- Upper lobe class function exponents, NU
- Lower lobe Class Functions, NL
- End of squashed lower lobe station, Station 1
- Start of circular lower lobe station, Station 2

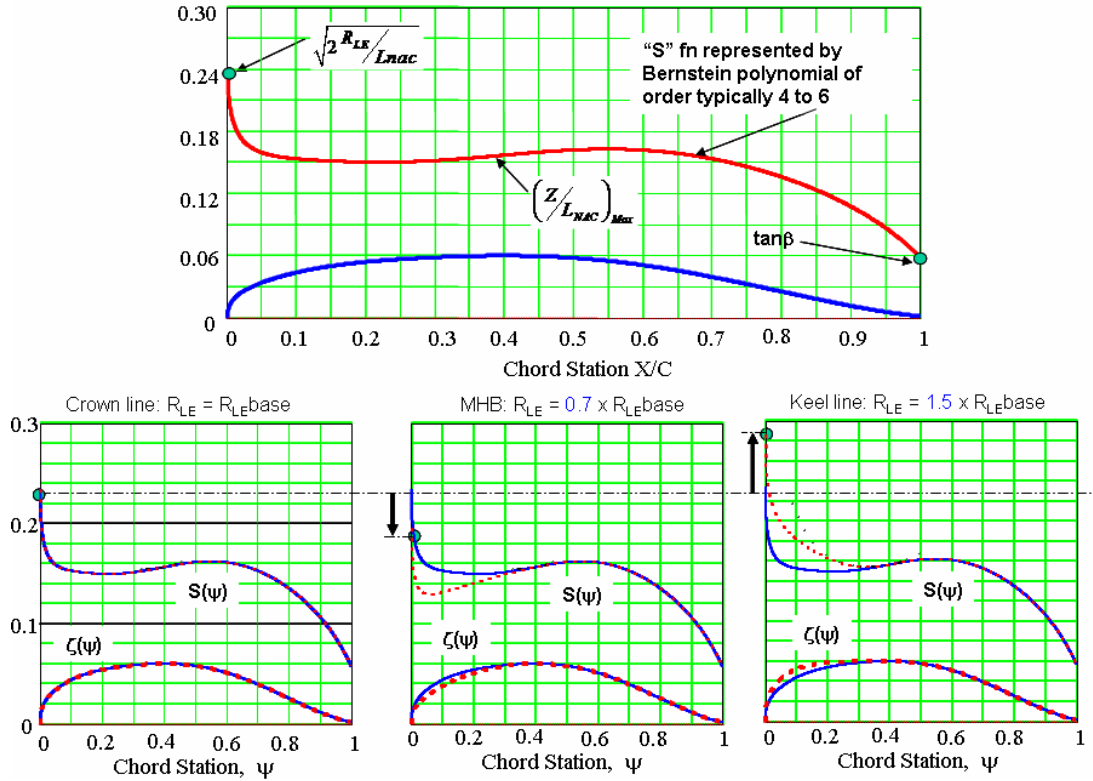


Figure 22: Nacelle Crown Line, Keel Line and Max Half Breadth Definitions → 8 Variables

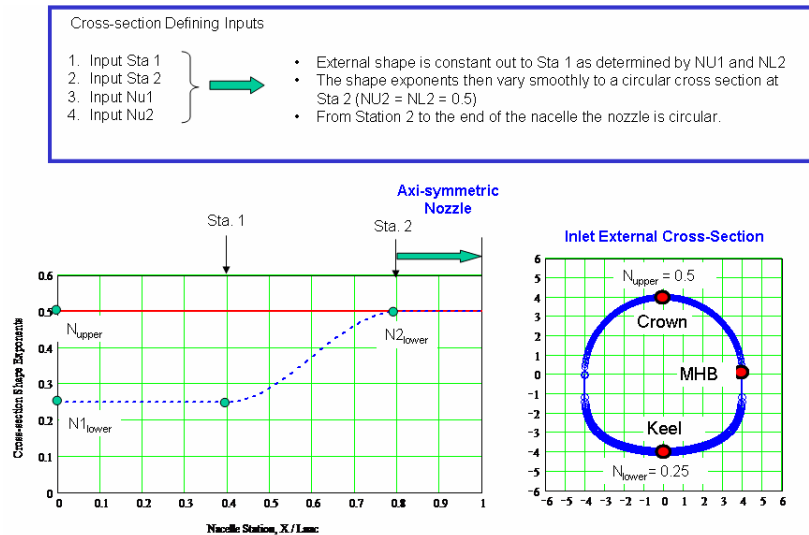


Figure 23: Nacelle Shape Distribution Circumferentially Around the Nacelle Centerline → 4 Variables

The inlet definition is shown in figure 24. The internal inlet cross-section shape and leading edge radii distribution were defined to match the external cowl cross-section shape and streamwise leading edge radius distribution at the nose of the nacelle.

The internal inlet shape morphed smoothly from the “squashed” shape at inlet lip to a circular cross-section at the throat station. The internal shape was defined as circular aft of the throat station to the end of the inlet length.

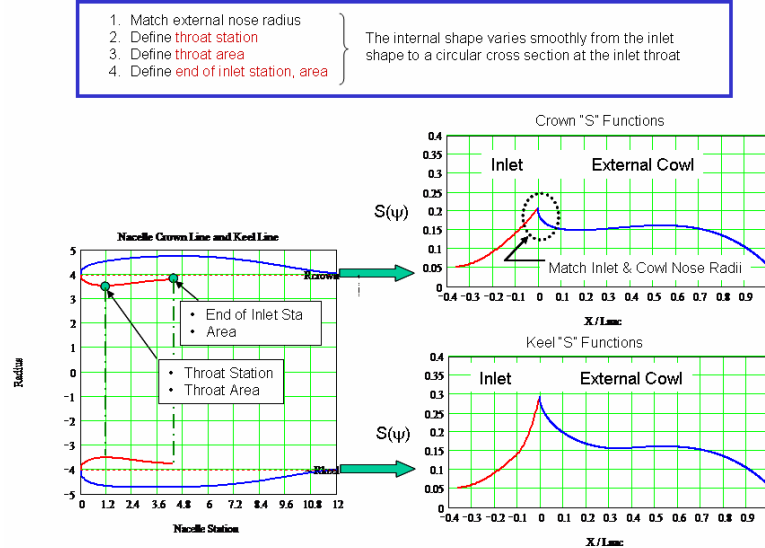


Figure 24: Nacelle Inlet Geometry Definition → 4 variables

The entire internal inlet geometry required only 4 more defining variables. These include:

- Throat Station
- Throat Area
- End of Inlet station
- End of Inlet area

The complete nacelle geometry as defined by the aforementioned 15 total nacelle design variables is shown in figure 25. The geometry is seen to be everywhere smooth and continuous.

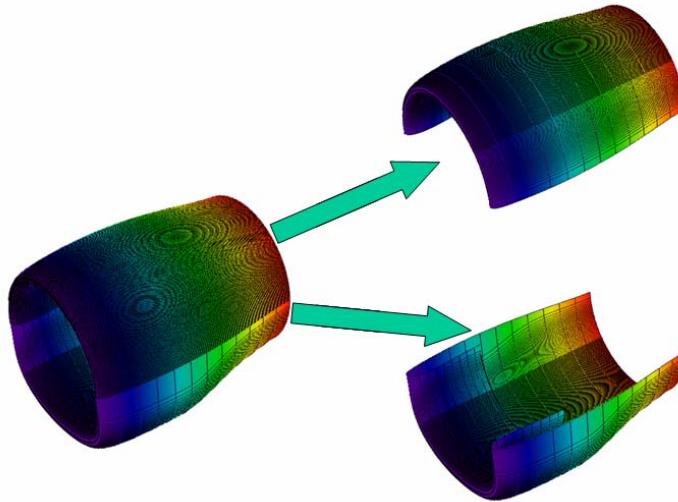


Figure 25: Total Nacelle External Shape and Inlet Geometry Definition → 15 variables

XI. 3D Wing Definition Using the CST Method

A 3D wing can be considered to be a distribution of airfoils across the wing span. Consequently we can use the previously discussed class functions and shape functions to obtain analytical definitions of the wing airfoil sections and then simply distribute the analytical formulations across the wing span to completely define a wing. In this section the general analytical definition for any arbitrary wing will be developed. We will illustrate the use the methodology initially with a number of simple applications. This will be followed by an examination of application of the methodology to detailed subsonic and supersonic wings definitions.

A 3D wing can be considered to be a distribution of airfoils across the wing span. Consequently we can use the previously discussed class functions and shape functions to obtain analytical definitions of the wing airfoil sections and then simply distribute the analytical formulations across the wing span to completely define a wing. In this section the general analytical definition for any arbitrary wing will be developed. We will illustrate the use the methodology initially with a number of simple applications. This will be followed by an examination of application of the methodology to detailed subsonic and supersonic wings definitions.

A typical wing airfoil section is shown in figure 26. The definition of a wing airfoil section has two additional parameters relative to the previously shown airfoil definition (figure 1)

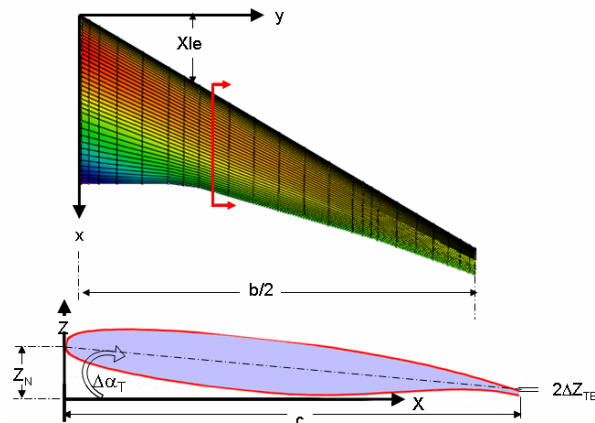


Figure 26: Wing Airfoil Section

The analytical definition of a local wing airfoil section is similar to the airfoil definition, (equation 1), with two additional parameters. That include the local wing shear and wing twist.

$$\zeta_U(\psi, \eta) = \zeta_N(\eta) + C_{1.0}^{0.5}(\psi) S_U(\psi, \eta) + \psi \left[\zeta_T(\eta) - \tan[\Delta\alpha_T(\eta)] \right] \quad (24)$$

Where:

Fraction of local chord:

$$\psi = \frac{x - x_{LE}(\eta)}{c(\eta)}$$

Non-dimensional semi-span station:

$$\eta = \frac{2y}{b}$$

Local leading edge coordinates:

$$x_{LE}(\eta)$$

Local chord length:

$$c(\eta)$$

Non-dimensional upper surface coordinate:

$$\zeta_U(\eta) = \frac{z_U(\eta)}{c(\eta)}$$

Non-dimensional local wing shear: $\zeta_N(\eta) = \frac{z_N(\eta)}{c(\eta)}$

Local wing twist angle: $\Delta\alpha_T(\eta)$

Equation 24 is the equation for the wing upper surface, the similar equation for the lower surface is:

$$\zeta_L(\psi, \eta) = \zeta_N(\eta) + C_{1.0}^{0.5}(\psi) S_L(\psi, \eta) + \psi [\zeta_T(\eta) - \tan[\Delta\alpha_T(\eta)]] \quad (25)$$

The physical z coordinate is transformed in the shape function using an extension of the airfoil shape function procedure to derive equation 2. The corresponding shape for an airfoil section on a wing with vertical shear and local section twist is given by the equation:

$$S_U(\psi, \eta) = \frac{\zeta_U(\psi, \eta) - \zeta_N(\eta) - \psi [\zeta_T(\eta) - \tan[\Delta\alpha_T(\eta)]]}{C_{1.0}^{0.5}(\psi)} \quad (26)$$

The corresponding shape function equation for the lower surface of a wing is:

$$S_L(\psi, \eta) = \frac{\zeta_L(\psi, \eta) - \zeta_N(\eta) - \psi [\zeta_T(\eta) - \tan[\Delta\alpha_T(\eta)]]}{C_{1.0}^{0.5}(\psi)} \quad (27)$$

For a given wing definition, the wing upper and lower shape functions can be calculated using above equations.

Given a wing definition as a shape function surface in the design space, the wing upper, and lower surfaces in physical space can be determined from the shape function surfaces, the local values of twist, shear and chord length as:

$$\begin{aligned} z_U(x, y) &= \left\{ \zeta_N(\eta) + C_{1.0}^{0.5}(\psi, \eta) S_U(\psi, \eta) + \psi [\zeta_T(\eta) - \tan[\Delta\alpha_T(\eta)]] \right\} C_{LOCAL}(\eta) \\ z_L(x, y) &= \left\{ \zeta_N(\eta) + C_{1.0}^{0.5}(\psi, \eta) S_L(\psi, \eta) + \psi [\zeta_T(\eta) - \tan[\Delta\alpha_T(\eta)]] \right\} C_{LOCAL}(\eta) \end{aligned} \quad (28)$$

A typical subsonic wing and the corresponding definition of the wing in the shape function design space is shown in figure 27. The unit design space is defined by $\psi = 0.0$ to 1.0 , and $\eta = 0.0$ to 1.0 and therefore represents any wing planform. As shown in the figure, the leading edges of the shape function surfaces define the leading edge radius distributions for the physical wing. The trailing edges of the shape function surfaces define the boat-tail angle distributions. The wing shape function surface shares the same desirable features as the shape function for an airfoil such as smooth, analytic, easily definable key geometric features.

The concept of the wing shape function surface can be used for many purposes including:

- Parametric wing definition
- Smoothing and / or enrichment of the wing geometry
- Local parametric changes of the wing geometry.
- Design optimization with local design point variables
- Regional design optimization such as the wing leading edge region.
- Global design optimization

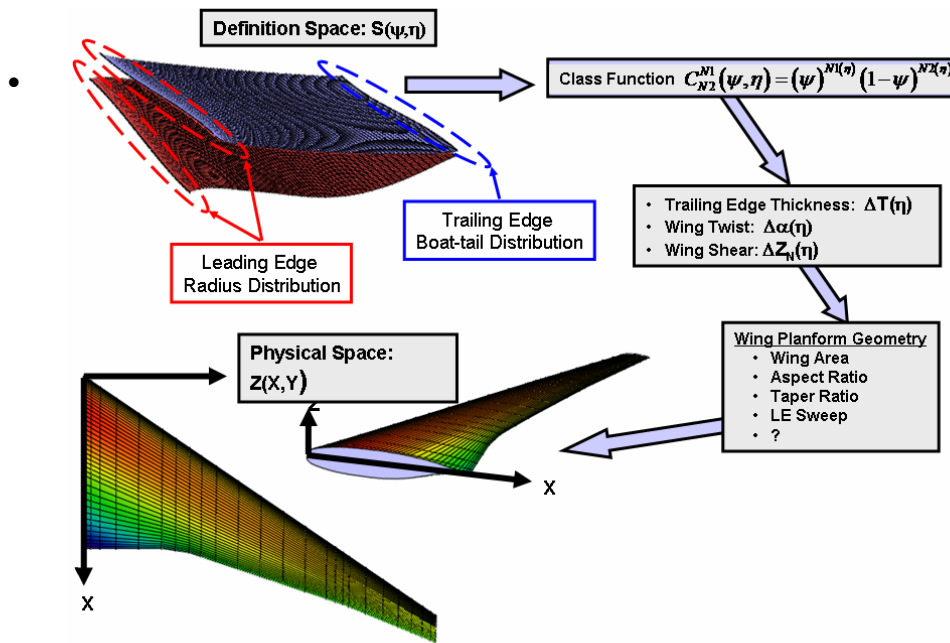


Figure 27 Definition of a wing in Design Space

Figure 28 illustrates the general process of transforming a simple parametric definition of shape function surfaces for a wing in design space into the physical definition of the wing.

The complete parametric cambered wing definition with spanwise variations of maximum thickness and wing twist, and specified wing area, sweep, aspect ratio and taper ratio required only a total of 19 design variables:

- Supercritical Airfoil Section (11)
- Spanwise Thickness Variation (2)
- Spanwise Twist Variation (2)
- Wing Area (1)
- Aspect Ratio (1)
- Taper Ratio (1)
- L.E. Sweep (1)

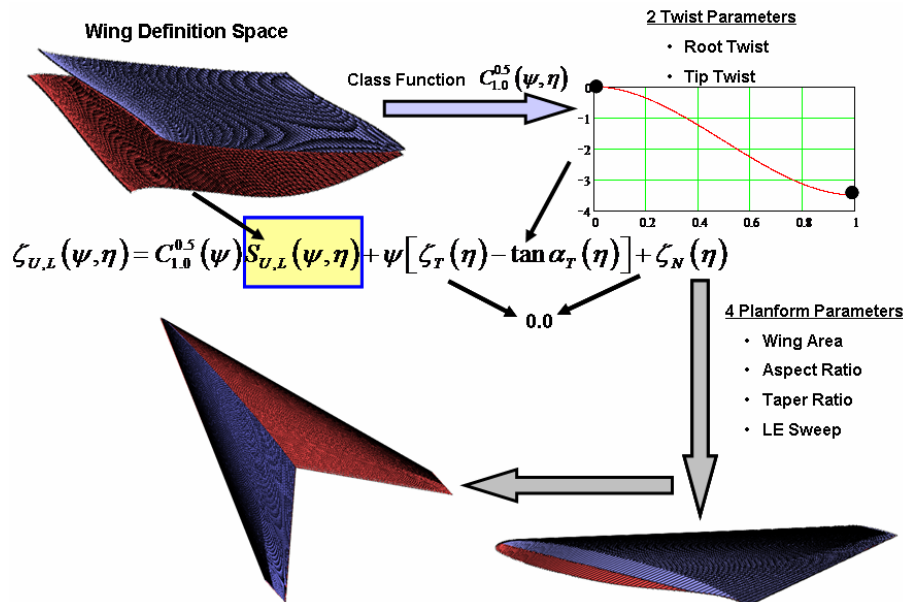


Figure 28 Complete Wing Analytic Definition

XII. Mathematical Description of a Wing in Design Space

Similar to the shape function for an airfoil, the shape function surface for wings such as shown in figure 28, is a smooth continuous analytic surface. Consequently the shape function surface can be described by a Taylor series expansion in x and y. It was shown in reference 2 that a Taylor series in x and y is equivalent to a Taylor series expansion first in the x direction, and then expanding each coefficient of the “x series” as a Taylor expansion in the y direction. In a similar manner, it can be shown that a power series in x and y is equivalent to an expansion in x followed by power series expansions in the y direction of each of the x series coefficients. Consequently, the shape function surface for a complete wing surface can be obtained by first representing the root airfoil shape function by a Bernstein polynomial of a specified order.

The complete wing shape function surface can then be defined by expanding the coefficients of the Bernstein in the spanwise direction using any appropriate numerical technique. The surface definition of the wing is then obtained by multiplying the shape function surface by the wing class function. This in essence provides a numeric scalar definition of the wing surface.

An example of the mathematical formulation of this process is shown below, using Bernstein polynomials to represent the stream wise airfoil shapes as well as for the spanwise variation of the streamwise coefficients.

The unit streamwise shape functions for Bernstein polynomial of order N_x are defined as:

$$Sx_i(\psi) = Kx_i \psi^i (1-\psi)^{N_x-i} \text{ for } i = 0 \text{ to } N_x \quad (29)$$

Where the streamwise binomial coefficient is defined as

$$Kx_i \equiv \binom{N_x}{i} \equiv \frac{N_x!}{i!(N_x-i)!} \quad (30)$$

The streamwise upper surface shape function at the reference spanwise station, η_{REF} is

$$Su(\psi, \eta_{REF}) = \sum_{i=1}^{N_x} Au_i(\eta_{REF}) Sx_i(\psi) \quad (31)$$

Let us represent the spanwise variation of each of the coefficients, $Au_i(\eta)$ by Bernstein polynomials as:

$$Au_i(\eta) = \sum_{j=1}^{N_y} Bu_{i,j} Sy_j(\eta) \quad (32)$$

Where $Sy_j(\psi) = Ky_j \eta^j (1-\eta)^{N_y-j} \text{ for } j = 0 \text{ to } N_y \quad (33)$

And $Ky_j \equiv \binom{N_y}{j} \equiv \frac{N_y!}{j!(N_y-j)!} \quad (34)$

The wing upper surface is then defined by:

$$\zeta_U(\psi, \eta) = \sum_i^{N_x} \sum_j^{N_y} Bu_{i,j} \{ C_{N2}^{N1}(\psi) Sy_j(\eta) Sx_i \} + \psi (\zeta_T(\eta) - \tan \alpha_{TWIST}(\eta)) + \zeta_N(\eta) \quad (35)$$

The similar equation for the lower surface is:

$$\zeta_L(\psi, \eta) = \sum_i^{N_x} \sum_j^{N_y} B_{l,i,j} \{C_{N2}^{N1}(\psi) S y_j(\eta) S x_i(\psi)\} + \psi (\zeta_T(\eta) - \tan \alpha_{TWIST}(\eta)) + \zeta_N(\eta) \quad (36)$$

In equations 35 and 36 the coefficients Bu_{ij} and Bl_{ij} define the unique geometry of the wing upper and lower surfaces. Continuity of curvature from the upper surface around the leading edge to the lower surface is easily obtained by the requirement: $Bu_{0,j} = Bl_{0,j}$

The actual wing surface coordinates can then be obtained from the equations:

$$\begin{aligned} y &= \frac{b}{2} \eta \\ x &= \psi C_{LOC}(\eta) + x_{LE}(\eta) \\ z_U(x, y) &= \zeta_U(\psi, \eta) C_{LOC}(\eta) \\ z_L(x, y) &= \zeta_L(\psi, \eta) C_{LOC}(\eta) \end{aligned} \quad (37)$$

This process of defining a wing geometry using equations 35, 36 and 37, may be considered a **scalar loft** of a wing where every points on the wing surface is defined as accurately as desired and the points are all “connected” by the analytic equations. This is in contrast to the usual wing definition of a **vector loft** of a wing which is defined as ordered sets of x,y,z coordinates plus “rules” that describe how to connect adjoining points. The common approach used to connect adjacent points is along constant span stations and along constant percent chord lines.

In equations 35 and 36, each term $\zeta_{ij}(\psi, \eta) = C_{N2}^{N1}(\psi) S y_j(\eta) S x_i(\psi)$ defines a composite wing geometry formed by the “ith” component airfoil shape $C_{N2}^{N1}(\psi) S x_i(\psi)$ with the ‘jth’ spanwise variation $S y_j(\eta)$. Figure 29 shows analytic wing components for an arrow wing with a Bernstein polynomial of order 3 for defining the basic airfoil shape and Bernstein polynomial of order 2 for describing the spanwise variations for each of the basic airfoil components. This results in a total of 12 component wing shapes used to define the complete wing geometry. Figure 30 shows three of the component wing shapes.

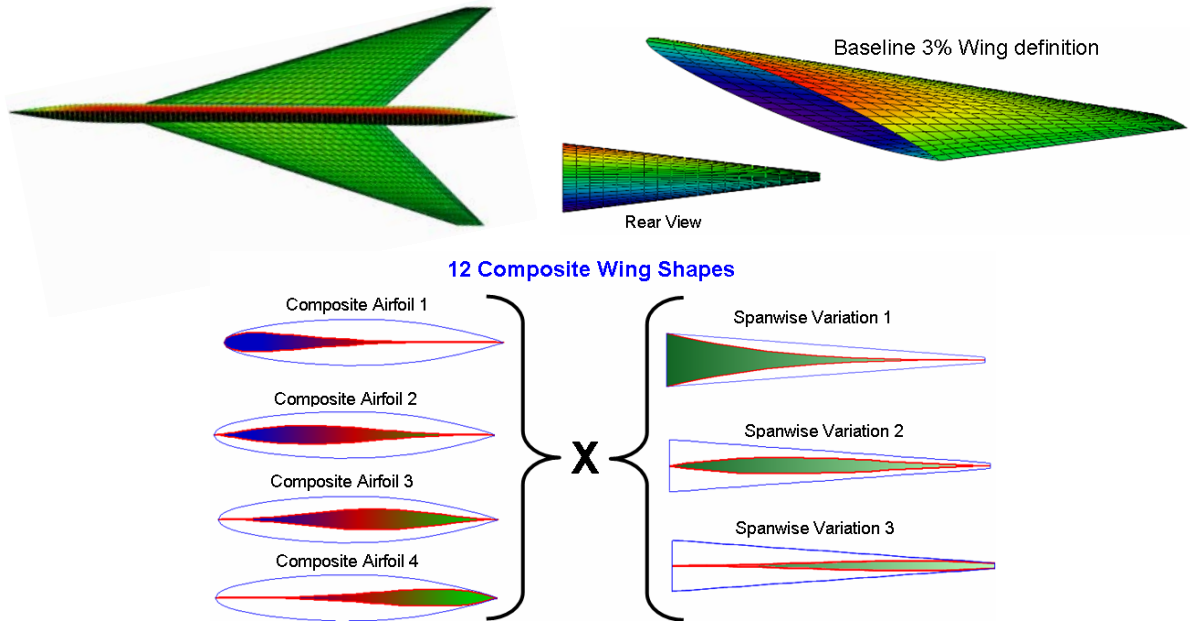


Figure 29: Arrow Wing Composite wing Elements Construction

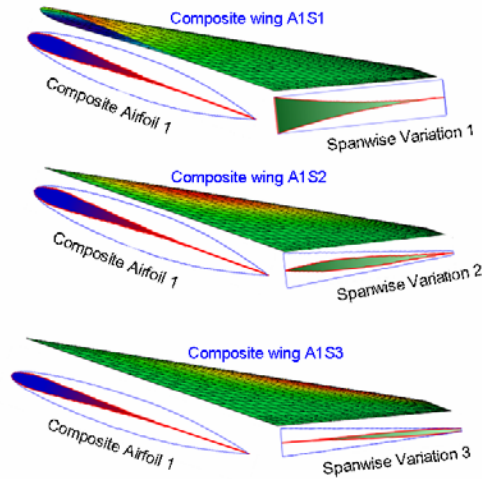


Figure 30: Example Composite Wing Elements

For a design optimization application, the 12 scaleable coefficients B_{ij} would be the optimization variables.

Figure 31 shows an example of a scalar loft of a highly swept wind tunnel configuration that was used to obtain surface pressure and wings loads data for CFD validation studies^{13, 14}. The wind tunnel model was built using the conventional vector loft approach.

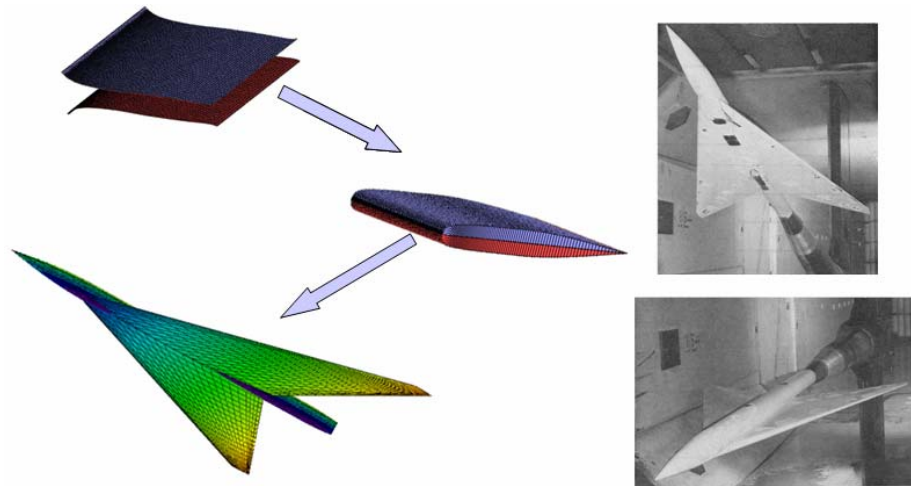


Figure 31: Scalar Loft of a Highly Swept Aero-elastic Loads Wind Tunnel Model

The analytic scalar loft of the wing was defined by a total of 15 parameters. These include:

- BPO8 representation of the basic airfoil section → 9 parameters
- Wing area
- Aspect ratio
- Taper ratio
- Leading edge sweep
- Trailing edge thickness = Constant
- Constant wing shear (to fit the wing on the body as a low wing installation)

The wind tunnel model fuselage included an ogive nose / cylindrical body. The ogive nose shape has distribution class function with exponents equal to 1 and a constant shape function equal to 4 times the maximum body radius. The total body geometry was specified by two variables that included the nose length and the maximum radius.

Body and wing surface coordinates were calculated using the aforementioned analytic definition. The differences between the analytic model surface definition and the “as built” wing surface coordinates were far less than wind tunnel model tolerances over the entire surface of the model.

XIII. Mathematical Description of a Wing With Leading Edge and /or Trailing Edge Breaks

Subsonic and supersonic aircraft wings typically have planform breaks in the leading edge (e.g. strake) and / or the trailing edge (e.g. yehudi) with discontinuous changes in sweep. Consequently, the wing surface is non-analytic in the local region of the edge breaks. However, the approach of defining a complete wing geometry as previously described should be piecewise applicable.

In order to explore this concept; the geometry of a typical subsonic aircraft wing was analyzed in depth. Airfoil sections at a large number of spanwise stations were approximated by equal order of Bernstein polynomial representation of the corresponding shape functions. The adequacy of the composite representation was determined by computing the residual differences between the actual airfoil sections and those defined by the approximating Bernstein polynomials. The wing upper and lower surface residual differences were well within the wind tunnel model construction tolerances.

The shape function surfaces corresponding to wing upper and lower surfaces are shown in figure 32. The piecewise continuous nature of the surfaces associated with the planform breaks is very evident. The corresponding spanwise variations of the composite airfoil scaling coefficients (Bu_i and Bl_i) are also shown.

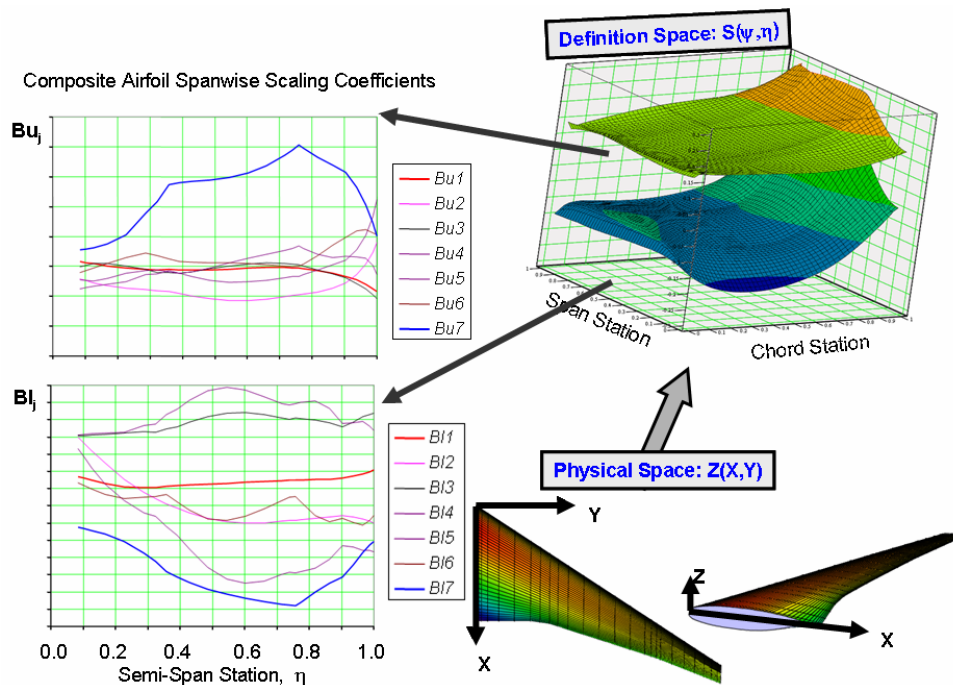


Figure 32: Spanwise Variation of the “BP” Composite Airfoil Scaling Coefficients

These results show that the spanwise variations of the Bernstein coefficients across the wing span are very regular, piecewise continuous and well behaved.

The shape function surface for a High Speed Civil Transport, Ref H, wing is shown in figure 33. This planform has a number of leading edge and trailing edge breaks. This wing has an inboard subsonic leading edge wing with round nose airfoils. Outboard of the leading edge the wing has a supersonic leading edge with sharp nose airfoils. The shape functions for this wing are also seen to be piecewise smooth and continuous.

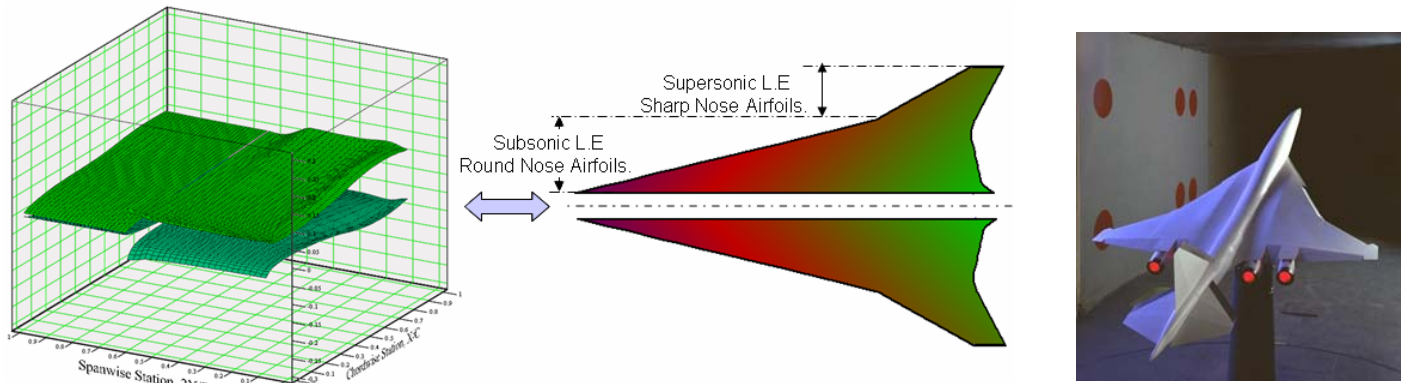


Figure 33: Shape Function for a HSCT Supersonic Wing – Ref H

The results shown in figures 32 and 33 imply indicate that analytic wing definitions for planforms with leading edge and / or trailing edge breaks, can be developed using streamwise airfoil components for a fixed order of Bernstein polynomials with piecewise variations of the polynomial coefficients in the spanwise direction.

XIV. Analytic Wing Global Design Optimization

In reference 15, a new supersonic linear theory wave drag optimization methodology utilizing far field wave drag methodology was introduced. The optimization process was used to explore wing design optimization with the class function / shape function transformation, CST, concept of an analytic scalar wing definitions.

Results of a simple application of the methodology for optimization of the spanwise thickness distribution of a supersonic delta wing at Mach 3.0 to minimize cruise volume wave drag, are shown in figures 34, 35 and 36.

The objective of the study was to explore the effect of the order of the order of the spanwise Bernstein polynomial representation of the wing shape function surface with a constant airfoil shape on wave drag with a constant wing volume. The basic wing / body geometry characteristics of the base configuration are shown in figure 34.

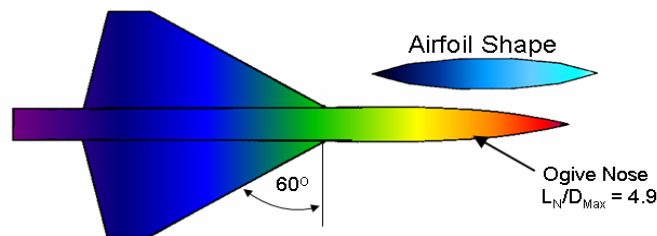


Figure 34: Basic Delta Wing / Body

Similar to the arrow wing analytic representation shown in figure 29, the study wing geometry was decomposed into scaleable component wing shapes formed by the different spanwise variations of the basic wing airfoil shape. The component wing shapes, corresponding to a 3rd order Bernstein polynomial describing the spanwise thickness variation, are shown in figure 35.

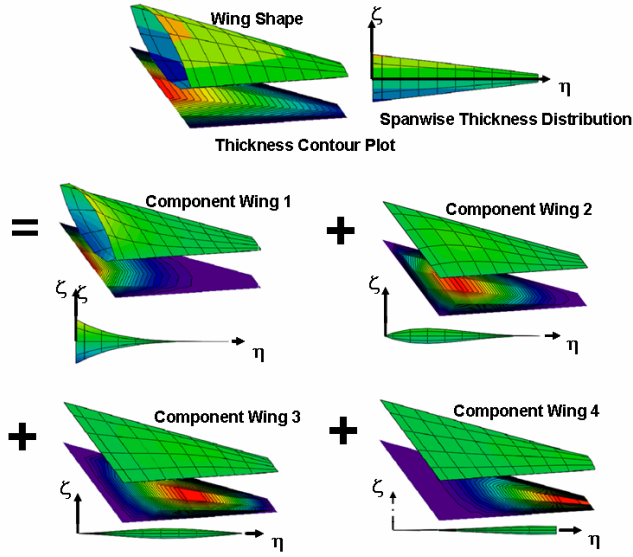


Figure 35 Example of BPO3 Spanwise Analytic Wing Components

Wing optimization studies were conducted with and with out outboard wing inequality thickness constraints. The thickness constraints limited the outboard thickness to no less than 1.1 %. In all cases the wing volume was held constant. Spanwise Bernstein polynomials of order, BPO 0 to 6 were utilized to define the composite wing shapes for the optimization studies. The results of the study are summarized in figure 36.

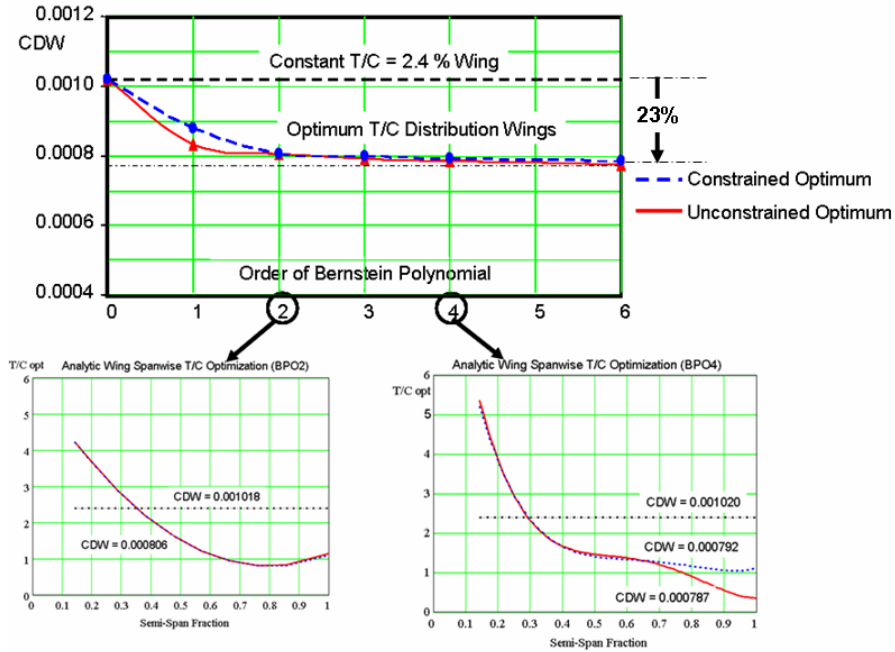


Figure 36: Effect of Spanwise Bernstein Polynomial order, BPO, on optimized wing wave drag.

The number of design optimization variables corresponding to scaling coefficients of the component wing shapes equals the BPO plus 1. The BPO = 0 result corresponds to the drag of the constant $T_{MAX}/C = 2.4\%$ baseline wing. It is seen that the wave drag rapidly converges to the minimum drag level when the BPO representation equals or exceeds 2. For this example the wing wave drag was reduced by 23%. Additional results of design optimization studies that demonstrate the effectiveness of the analytic optimization methodology using composite wings representing both airfoil shape and spanwise thickness variations over the wing surface are shown in reference 15.

XV. Summary and Conclusions

Figure 37 summarizes the evolution of the CST method as presented in this report.

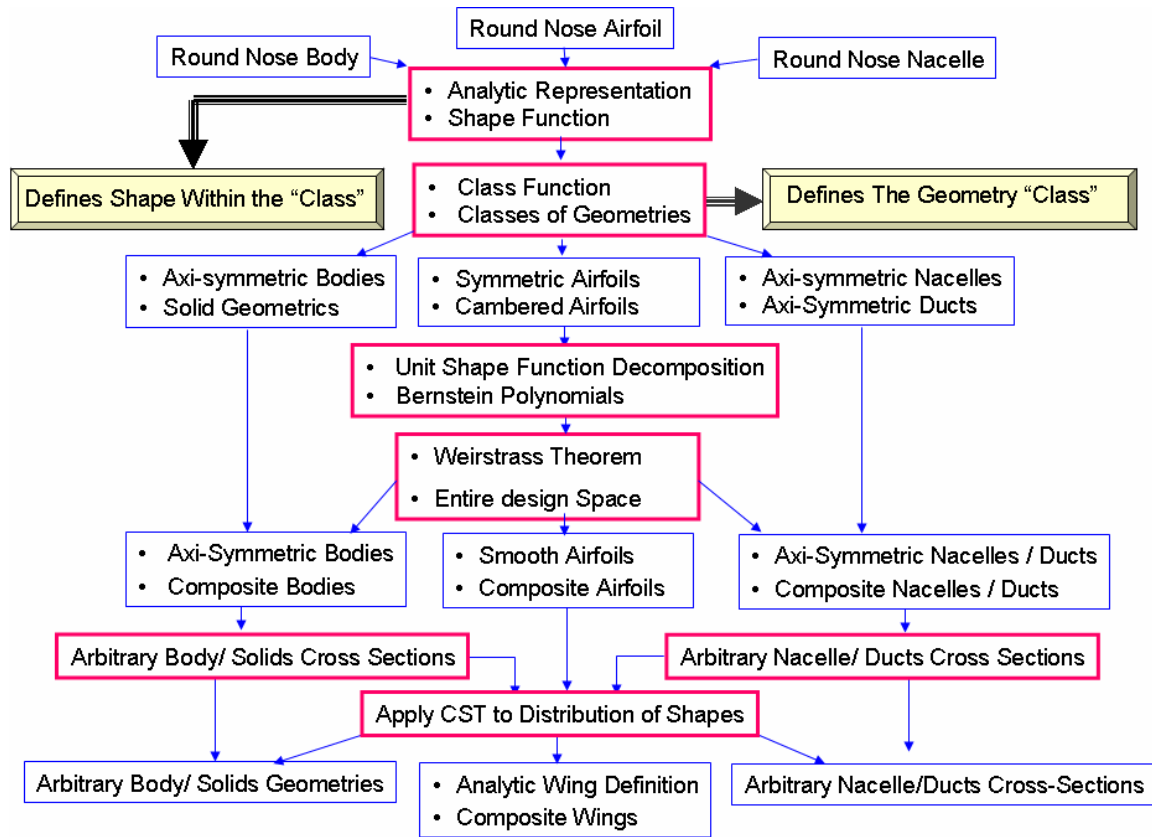


Figure 37: Evolution of the CST Method

- The concept of the “SHAPE FUNCTION” was developed by a transformation process that eliminated the numerical leading edge singularities in slopes, 2nd derivatives and the large variations in curvature over the entire surface of an airfoil. In addition, the shape function provides direct control of key design parameters such as leading edge radius, continuous curvature around a leading edge, boat-tail angle and closure to a specified thickness.
- The transformation process was generalized with the introduction of the “CLASS FUNCTION”.
- The class function defines fundamental classes of airfoils, axi-symmetric bodies, and axi-symmetric nacelles geometries. The shape function defines unique geometric shapes within each fundamental class.
- The unit shape function was decomposed into component airfoils using Bernstein Polynomials. This is an attractive and systematic technique to decompose the basic unit shape into scalable elements corresponding to discrete component airfoils.
- By virtue of the Weirstrass theorem it was shown that this technique:
 - Captures the entire design space of smooth airfoils, axi-symmetric bodies and nacelles
 - Within this design space, all smooth airfoils, axi-symmetric bodies and nacelles are derivable from the unit shape function and therefore from each other.

- Very detailed geometric and aerodynamic evaluations were made of approximate airfoil geometries derived from various orders of Bernstein polynomials representations of the shape functions for a wide variety of airfoil geometries. The results indicated that relatively few variables were required to accurately represent most any airfoil geometry.
- The CST methodology can be readily adapted to describe both warping and morphing of geometric components. Geometric morphing can be easily obtained by variations of class function / shape function variables. Warping involves geometric variations external to the class function / shape function variables.
- The Class function / Shape function Transformation geometry representation methodology, CST, can be used to describe both the cross-sectional shapes of arbitrary bodies or nacelles as well as the distribution of the cross-section shapes along the primary body axis. This provides a powerful technique to smoothly morph a three dimensional geometry into widely differing configuration.
- The concept of “analytic scalar definitions using composite wing surfaces” was introduced and explored. With this approach, the wing airfoil shapes functions are represented by a Bernstein polynomial. The selected order of Bernstein polynomial effectively defines a set of composite airfoils. The scalable coefficients of the composite airfoils can then be mathematically expanded in the spanwise direction to define a set of composite wing shapes.
- The complete wing upper and lower shape function surfaces can then defined by scaling the set of composite wing shapes as the variables for design optimization applications and parametric design studies.

The concept of the wing shape function surface can be used for many purposes including:

- Parametric wing and body definitions
- Smoothing and / or enrichment of the wing or body geometries.
- Local parametric changes of the wing geometry.
- Defining seeming complex geometries with relatively few variables
- Aerodynamic and multi-disciplinary design optimization, MDO, studies with relatively few required design variables
- Local area design optimization such as the wing leading edge region.
- The analytic CST geometry representation methodology presented in this report provides a unified and systematic approach to represent a wide variety of 2D and 3D geometries encompassing a very large design space with a relatively few scalar parameters.

XVI. References

1. Kulfan, B. M, Bussoletti, J. E., "'Fundamental Parametric Geometry Representations for Aircraft Component Shapes". AIAA-2006-6948, 11th AIAA/ISSMO Multidisciplinary Analysis and Optimization Conference: The Modeling and Simulation Frontier for Multidisciplinary Design Optimization, 6 - 8 September, 2006
2. Kulfan, B. M., "Universal Parametric Geometry Representation Method – "CST", AIAA-2007-0062, 45th AIAA Aerospace Sciences Meeting and Exhibit , January, 2007
3. Sobieczky, Helmut, "Aerodynamic Design and Optimization Tools Accelerated by Parametric Geometry Preprocessing ", , European Congress on Computational Methods in Applied Sciences and Engineering, ECCOMAS 2000
4. Sobieczky, H., "Parametric Airfoils and Wings, "Notes on Numerical Fluid Mechanics", Vol. 68, pp.71-88, Vieweg Verlag, 1998
5. Samareh, J.A., "Survey of Shape Parameterization Techniques for High-Fidelity Multidisciplinary Shape Optimization", AIAA JOURNAL Vol. 39, No. 5, May 2001
6. Robinson, G. M., and Keane, A. J., "Concise Orthogonal Representation of Supercritical Airfoils", Journal of Aircraft, Vol. 38, NO. 3
7. Song, W., and Keane, A.J., "A Study of Shape Parameterization Airfoil Optimization", AIAA-2004-4482 10th AIAA/ISSMO Multidisciplinary Analysis and Optimization Conference, Albany, New York, Aug. 30-1, 2004
8. Padula, S., and Li, W., "Options for Robust Airfoil Optimization Under Uncertainty", 9th AIAA Multidisciplinary Analysis and Optimization Symposium, 4-6 September 2002
9. Hicks, R. M. and Henne, P. A., "Wing design by numerical optimization", Journal of Aircraft, Vol. 15, pp. 407-412, 1978.
10. Padula, S., and Li, W., "Options for Robust Airfoil Optimization Under Uncertainty", 9th AIAA Multidisciplinary Analysis and Optimization Symposium, 4-6 September 2002
11. Timothy W. Purcell, T. W., and Om, D., "TRANAIR Packaging for Ease-of-Use in Wing Design", AIAA-1998-5575, AIAA and SAE, 1998 World Aviation Conference, Anaheim, CA, Sept. 28-30, 1998
12. Samant, S. S., Bussoletti, J. E., Johnson, F. T., Burkhart, R. H., Everson, B. L., Melvin, R. G., Young, D. P., Erickson, L. L., and Madson, M. D., "TRANAIR - A Computer Code for Transonic Analyses of Arbitrary Configurations", AIAA-1987-34, Aerospace Sciences Meeting, 25th, Reno, NV, Jan 12-15, 1987
13. Manro, M.E., Percy J. Bobbitt, P.J. and Kulfan, R. M., "The Prediction of Pressure Distributions on an Arrow Wing Configuration Including the effects of Camber Twist and a Wing Fin", NASA CP-2108 Paper No 3 pages 59 to 115, November 1979
14. Wery, A.C., and Kulfan, R. M., "Aeroelastic Loads Prediction for an Arrow Wing - Task II Evaluation of Semi-Empirical Methods", NASA CR-3641 March 1983
15. Kulfan, B. M., "A New Supersonic Wing Far-Field Composite Element Wave Drag Optimization Method, "FCE"", AIAA-2008-0132, 46th AIAA Aerospace Sciences Meeting and Exhibit , January, 2008